Interference Cancellation Matrix Beamforming for 3-D Beamspace ML/MUSIC Bearing Estimation

Michael D. Zoltowski, *Member, IEEE,* and Ta-Sung Lee, *Member, IEEE*

Abstract—**In conventional monopulse radar, the bearing of a single target within the mainlobe of the transmitted beam is estimated via a ML procedure based in a 2-D beamspace defined by sum and difference beams. For the case of two closely spaced targets angularly located within the mainlobe of the transmitted beam, 3D-BDML is a computationally simpie ML bearing estimation scheme which operates in a 3-D beamspace generated by three orthogonal, classical beamformers. The presence of strong interferers angularly located outside the mainlobe encompassing the two targets of interest necessitates the use of adaptively formed left, center, and right beams. Let M denote the number of elements comprising the array. Novel procedures are developed for the construction of an $M \times 3$ interference cancellation matrix beamformer which retains those properties of the $M \times 3$ classical matrix beamformer critical to the computational simplicity of 3D-BDML. The most important of these is commonality of $M - 3$ nulls among the left, center, and right beams. Simulations are presented demonstrating the excellent performance of both single frequency and multifrequency 3D-BDML incorporating interference cancellation in a simulated low-angle radar tracking environment.**

I. Introduction

In conventional monopulse radar, the bearing of a single target within the mainlobe of the transmitted beam is estimated via a ML procedure based in a 2-D beamspace defined by sum and difference beams [2], [3]. In the presence of strong interference, the sum and difference beams are formed adaptively such that ideally each exhibits a null in the direction of each and every interferer [2], [3]. Judicious construction of the adaptive sum and difference beams enables one to nullify the effect of interferers and nevertheless estimate the target bearing from the monopulse ratio of the difference beam output to the sum beam output in a very simple manner [3]. If an interfering source is angularly located within a beamwidth of the target being tracked, however, it is well known that the performance of the adaptive sum and difference beam method degrades severely. In attempting to place a null in the angular location of the interferer, the pointing angle of the sum beam, and hence, the direction of maximum gain, squints away from the angular position of the target under surveillance. As the angular separation between the target and the interferer becomes a smaller and smaller fraction of a beamwidth, the drop in target SNR at the adaptive sum beam output becomes more and more severe. The target SNR at the adaptive difference beam output is affected similarly. Ultimately this phenomenon causes track breaking.

The low-angle radar tracking problem [1], [4]–[10] is a classical example of a mainbeam interference problem. In low-angle radar tracking, echoes return from a target angularly located near broadside to a vertical array via a specular path as well as by a direct path. The specular path signal arises due to the relative proximity of both the target and the array to a smooth reflecting surface. Due to the low elevation angle of the target, the direct and specular path signals arrive within a fraction of a beamwidth near broadside. The specular path signal thus represents an interfering signal angularly located within a beamwidth of the signal of interest, the direct path signal. It should be noted that the differential between the direct and specular path lengths is small enough such that the two respective signals arrive overlapping in time. As a consequence, the two cannot be distinguished according to range bin.

Rather than attempting to place a null in the direction of the specular path signal, it is apparent that it must be treated as arising from a second source located at the image of the target. The bearing estimation problem in low-angle radar tracking then represents a classical example of a real world problem in which it is necessary to resolve two sources angularly separated by less than the 3-dB beamwidth of the radar array pattern. As single target tracking is accomplished very simply and very effectively in a 2-D beamspace, a number of bearing estimation schemes based in a suitably defined 3-D beamspace have been proposed for the low-angle radar tracking problem [4]–[7]. The 3D-BDML [9], [10], [12] is a computationally simple ML-based bearing estimation algorithm developed for low-angle radar tracking which operates in a 3-D beamspace generated by an $M \times 3$ Butler matrix beamformer composed of three orthogonal, classical beamformers with equispaced pointing angles. Here M denotes the number of elements comprising the array assumed to be linear and equispaced. The computational simplicity of 3D-BDML is primarily due to judicious ex-

Manuscript received March 28, 1990; revised August 21, 1990. This work was supported by the National Science Foundation under Grant ECS-8707681 and by a grant from the Corporate Research and Development Center of the General Electric Company.

M. D. Zoltowski is with the School of Electrical Engineering, Purdue University, West Lafayette, IN 47907.

T.-S. Lee is with the Department of Communication Engineering, National Chiao Tung University, Hsinchu, Taiwan, Republic of China.

IEEE Log Number 9100760.

ploitation of the fact that the corresponding left, center, and right beams have $M - 3$ nulls in common.

The presence of strong interferers (other than the specular path signal) angularly located outside the angular region encompassed by the mainlobes of the left, center, and right beams used to monitor the direct and specular path signals in low-angle radar tracking necessitates the use of adaptively formed left, center, and right beams. It is shown within that judicious construction of an $M \times 3$ interference cancellation matrix beamformer enables one to nullify the effect of interferers and nevertheless estimate the respective bearings of the direct and specular path signals via the computationally simple 3D-BDML algorithm with minor modification. The major contribution within is the development of novel procedures for constructing the $M \times 3$ interference cancellation matrix beamformer such that those properties of $M \times 3$ Butler matrix beamforming critical to the computational simplicity of 3D-BDML are preserved. The critical properties are orthonormality and conjugate centrosymmetry among the columns, i.e., the left, center, and right beamforming vectors, and, most importantly, commonality of $M - 3$ nulls among the three respective beam patterns. These properties facilitate estimation of the respective bearings of the direct and specular path signals via the roots of a quadratic equation whose coefficients are simple functions of the components of the "smallest" eigenvector of a 3×3 real-valued beamspace correlation matrix. These new matrix beamforming procedures also facilitate the formulation of a computationally simple version of 3D-BDML which incorporates frequency diversity as well as interference cancellation.

The description of the 3D-BDML algorithm may sound more like the description of a MUSIC algorithm [17] based in a 3-D beamspace. In fact, in the special case of only two (closely spaced) sources and Gaussian distributed receiver noise, the 3-D beamspace domain MUSIC (3D-BDMUSIC) algorithm is the ML estimator when the data is the 3-D beamspace domain snapshot vectors formed by the $M \times 3$ Butler matrix beamformer [10], [12]. Of cource, this yields different estimates than the ML estimator based in element space. When interference is present and measures are taken to nullify this interference, however, it is no longer strictly valid to refer to the algorithm as a maximum likelihood procedure. Hence, for the remainder of this paper, 3D-BDML will be referred to as 3D-BDMUSIC and when employing an interference cancellation matrix beamformer, the algorithm will be referred to as 3D-BDMUSIC incorporating interference cancellation.

Although the low-angle radar tracking problem is the motivating application, the bearing estimation procedures presented within are developed for the more general case in which two targets closely spaced in both angle and range give rise to respective echoes which arrive overlapping in time and angularly separated by less than a beamwidth. That is, the method developed herein does not require that the two closely spaced targets being tracked at a given instant in time be located near broadside. It is proposed that the 3-D beamspace techniques developed here be utilized in the same manner in which adaptive sum and difference beams are varied from one pointing angle to another in the process of sequentially tracking a large number of targets.

This paper is organized as follows. Section II introduces simplifying notation, defining the polynomial and vector representations of a causal sequence. The matrix formulation of linear convolution critical to later developments is presented as well. Section III briefly reviews the 3D-BDMUSIC algorithm for estimating the respective bearings of two closely spaced targets emphasizing those properties of $M \times 3$ Butler matrix beamforming critical to the computational simplicity of the algorithm. Section IV develops a minimum variance distortionless response (MVDR) based procedure for constructing the $M \times 3$ interference cancellation matrix beamformer which preserves these properties and, hence, the computational simplicity of 3D-BDMUSIC. A multifrequency version of 3D-BDMUSIC incorporating interference cancellation is presented in Section V which retains the computational simplicity of single frequency operation via coherent signal subspace processing according to the method of Wang and Kaveh [13], [14]. The coherent signal subspace processing of the multifrequency data also gives rise to a large effective signal-to-interference plus noise ratio (SINR) and reduces the sensitivity of 3D-BDMUSIC to the phase difference between the respective echo returns from the two closely spaced targets at any one frequency. Finally, simulations are presented in Section VI demonstrating the excellent performance of both single frequency and multifrequency 3D-BDMUSIC incorporating interference cancellation in a simulated low-angle radar tracking environment with strong jamming.

II. Notation and Matrix Representation of Linear Convolution

We here introduce notation which will be invoked throughout. Let $p(z)$ be a polynomial of order $L - 1$ defined as

$$p(z) = p_0 + p_1 z + p_2 z^2 + \cdots + p_{L-1} z^{L-1}. \quad (2.1a)$$

$\{\boldsymbol{p}\}$ then represents a causal sequence of length L expressed as

$$\{\boldsymbol{p}\} = \{p_0, p_1, p_2, \cdots, p_{L-1}\}. \quad (2.1b)$$

Finally, $\boldsymbol{p}$ represents the $L \times 1$ coefficient vector associated with $p(z)$ constructed as

$$\boldsymbol{p} = [p_0, p_1, p_2, \cdots, p_{L-1}]^T. \quad (2.1c)$$

Thus, as long as one of these entities is defined, the other two are defined automatically.

In this notational convention, let $\boldsymbol{q}$ be an $M \times 1$ vector defined similar to $\boldsymbol{p}$ in (2.1c). This automatically defines $q(z)$, a polynomial of order $M - 1$, and $\{\boldsymbol{q}\}$, a causal sequence of length M. Let $r(z)$ be the product of $p(z)$ and

$q(z)$, i.e., $r(z) = p(z)\,q(z)$, a polynomial of order $N = M + L - 2$. Of course, the set composed of the roots of $r(z)$ is equal to the union of the set composed of the roots of $p(z)$ with the set composed of the roots of $q(z)$. Also, the sequence $\{r\}$ is the linear convolution of the sequence $\{p\}$ with the sequence $\{q\}$, i.e.,

$$r_n = \sum_{k=0}^{L-1} p_k q_{n-k} = \sum_{k=0}^{M-1} q_k p_{n-k}$$
$$n = 0, 1, \cdots, M + L - 2. \quad (2.2)$$

As indicated, $\{r\}$ is a sequence of length $N = M + L - 1$. We thus have the following polynomial, sequence, and vector representations associated with either the product of two polynomials or, equivalently, the linear convolution of two causal sequences:

$$r(z) = p(z)\,q(z) \quad (2.3a)$$
$$\{r\} = \{p\} * \{q\} \quad (2.3b)$$
$$\begin{bmatrix} r_0 \\ r_1 \\ r_2 \\ \vdots \\ r_{M+L-2} \end{bmatrix} = \begin{bmatrix} p_0 & 0 & 0 \\ p_1 & p_0 & 0 \\ \vdots & \vdots & \vdots \\ p_{L-1} & p_{L-2} & 0 \\ 0 & p_{L-1} & 0 \\ 0 & 0 & p_0 \\ \vdots & \vdots & \vdots \\ 0 & 0 & p_{L-1} \end{bmatrix} \begin{bmatrix} q_0 \\ q_1 \\ q_2 \\ \vdots \\ q_M \end{bmatrix}. \quad (2.3c)$$

Note that the matrix representation of linear convolution in (2.3c) follows from the definition of linear convolution in (2.2). For notational simplicity, we will find it convenient in the development within to express (2.3c) in compact form as

$$\boldsymbol{r} = \begin{bmatrix} \boldsymbol{p} & 0 & 0 \\ 0 & \boldsymbol{p} & 0 \\ 0 & 0 & 0 \\ \vdots & \vdots & \vdots \\ 0 & 0 & \boldsymbol{p} \end{bmatrix} \boldsymbol{q} \quad (2.4)$$

where it is understood that (2.4) is shorthand for (2.3c).

III. Overview of 3D-BDMUSIC Algorithm with $M \times 3$ Butler Matrix Beamforming

A. Array Signal Model

It is assumed throughout that the two closely spaced targets of interest are either in the far field or that far-field focusing is accomplished by correcting for the quadratic phase curvature associated with a specific range bin under scrutiny. In addition, we here assume the radar array employed to be linear and composed of M elements uniformly spaced by half the wavelength of the transmitted pulse. Let $\boldsymbol{x}(n)$ denote the $M \times 1$ snapshot vector. The mth element of $\boldsymbol{x}(n)$, denoted $x_m(n)$, $m = 1, \cdots, M$, is the value of the complex analytic signal outputted from the mth element of the array measured at discrete time n. Invoking the narrowband model, $\boldsymbol{x}(n)$ may be expressed as

$$\boldsymbol{x}(n) = A_1(n)\, e^{j\phi_1(n)} \boldsymbol{a}(u_1; M) + A_2(n)\, e^{j\phi_2(n)} \boldsymbol{a}(u_2; M) + \boldsymbol{i}(n) + \boldsymbol{n}(n) \quad n = 1, \cdots, N$$
$$= [\boldsymbol{a}(u_1; M) \vdots \boldsymbol{a}(u_2; M)] \begin{bmatrix} A_1(n) e^{j\phi_1(n)} \\ A_2(n) e^{j\phi_2(n)} \end{bmatrix} + \boldsymbol{i}(n) + \boldsymbol{n}(n)$$
$$= \boldsymbol{A}\boldsymbol{c}(n) + \boldsymbol{i}(n) + \boldsymbol{n}(n). \quad (3.1)$$

The various quantities are defined. $u_i = \sin\theta_i$, $i = 1, 2$, where θ_i denotes the arrival angle of the ith signal with respect to broadside. $A_i(n)$ and $\phi_i(n)$, $i = 1, 2$, denote the magnitude and phase of the sample value of the complex envelope associated with the ith signal arrival at the nth snapshot. In the low-angle radar tracking scenario, one of the indices, $i = 1, 2$, is associated with the direct path signal while the other is associated with the specular path signal. The components of $\boldsymbol{i}(n)$ represent the interference present at each of the array elements at the nth snapshot due to external sources such as jammers and clutter. The components of $\boldsymbol{n}(n)$ represent the complex, receiver generated noise present at each of array elements at the nth snapshot. It is here assumed that the components of $\boldsymbol{n}(n)$ are independent with zero means and identical variances. As $\phi_i(n)$ is the phase of the ith signal occurring at the center of the array aperture at the nth snapshot, $\boldsymbol{a}(u_i; M)$ accounts for a linear phase variation across the array due to the far field assumption:

$$\boldsymbol{a}(u; M) = \left[\exp\left(-j\pi \frac{M-1}{2} u\right), \exp\left(-j\pi \frac{M-3}{2} u\right), \cdots, \exp\left(j\pi \frac{M-3}{2} u\right), \exp\left(j\pi \frac{M-1}{2} u\right)\right]^T. \quad (3.2)$$

The notation $\boldsymbol{a}(u; M)$ is such that M designates the dimension of the vector. Note that if M is odd the center element of $\boldsymbol{a}(u; M)$ is unity.

Note that when $\boldsymbol{a}(u; M)$ for some specific value of u is employed as a weight vector applied to $\boldsymbol{x}(n)$, the operation is referred to as classical beamforming. Consider the $M \times 3$ beamforming matrix

$$\boldsymbol{W}_B = \left[\boldsymbol{a}\left(u_c - \frac{2}{M}; M\right) \vdots \boldsymbol{a}(u_c; M) \vdots \boldsymbol{a}\left(u_c + \frac{2}{M}; M\right)\right]$$
$$= [\boldsymbol{w}_{BL} \vdots \boldsymbol{w}_{BC} \vdots \boldsymbol{w}_{BR}] \quad (3.3)$$

u_c is the pointing angle of the "center" beam. u_c may be the direction of the transmitted pulse or determined by geometrical considerations. For example, in a low-angle radar tracking scenario, $u_c = 0$. In any event, in order to achieve adequate SNR's at the beamspace ports, u_c should be determined in some judicious fashion so as to be in the general angular vicinity of the targets being tracked at a given instant in time. $u_c - (2/M)$ and $u_c + (2/M)$ are the pointing angles of the "left" and "right" beams, respectively. Correspondingly, for notational simplicity, the first, second, and third columns of $\boldsymbol{W}_B$ will alternatively be denoted as $\boldsymbol{w}_{\mathrm{BL}}$, $\boldsymbol{w}_{\mathrm{BC}}$, and $\boldsymbol{w}_{\mathrm{BR}}$, respectively, in accordance with the far right-hand side of (3.3). This automatically defines the $(M-1)$th order polynomials $w_{\mathrm{BL}}(z)$, $w_{\mathrm{BC}}(z)$, and $w_{\mathrm{BR}}(z)$ in accordance with (2.2). The subscript B is in reference to the Butler matrix beamformer. The Butler matrix beamformer for an M element array is an $M \times M$ matrix composed of M orthogonal, classical beamforming vectors of the form in (3.2); the corresponding pointing angles are integer multiples of $2/M$ covering the "visible" region $-1 \leq u \leq 1$. The Butler matrix beamformer is, in fact, an M pt. DFT matrix. For the purposes of this paper, we will refer to $\boldsymbol{W}_B$ defined by (3.3) as the $M \times 3$ Butler matrix beamformer despite the fact that u_c need not be an integer multiple of $2/M$. It is easily shown that the three columns of $\boldsymbol{W}_B$ are mutually orthogonal due to the $2/M$ spacing between the beams.

Note that $\boldsymbol{a}(u; M)$ exhibits conjugate centrosymmetry, i.e.,

$$\tilde{\boldsymbol{I}}_M \boldsymbol{a}(u; M) = \boldsymbol{a}^*(u; M) \tag{3.4}$$

where $\tilde{\boldsymbol{I}}_M$ is the $M \times M$ reverse permutation matrix

$$\tilde{\boldsymbol{I}}_M = \begin{bmatrix} 0 & 0 & \cdots & 1 \\ 0 & 0 & \cdots & 0 \\ \vdots & \vdots & \ddots & \vdots \\ 0 & 1 & \cdots & 0 \\ 1 & 0 & \cdots & 0 \end{bmatrix}. \tag{3.5}$$

Thus, each of the three columns of $\boldsymbol{W}_B$ is conjugate centrosymmetric. This property is invoked in the 3D-BDMUSIC method to be described shortly. Note that $\tilde{\boldsymbol{I}}_M \tilde{\boldsymbol{I}}_M = \boldsymbol{I}_M$, where $\boldsymbol{I}_M$ is the $M \times M$ identity matrix. Also, $\tilde{\boldsymbol{I}}_M^T = \tilde{\boldsymbol{I}}_M$. These properties of $\tilde{\boldsymbol{I}}_M$ will be invoked throughout.

An algorithmic summary of 3D-BDMUSIC is delineated below. A brief discussion of each step is provided to emphasize three important properties of the $M \times 3$ Butler matrix beamformer defined in (3.3) which contribute greatly to the computational simplicity of the algorithm. The reader is referred to [10], [12] for the full development of the algorithm. It should be noted that this version of the algorithm assumes the contribution to the beamspace snapshot vector due to interference to be negligible with respect to the contribution due to the signals of interest, i.e., $\|\boldsymbol{W}_B^H \boldsymbol{i}(n)\|_2 << \|\boldsymbol{W}_B^H \boldsymbol{A}\boldsymbol{c}(n)\|_2$. This assumes that the interference is not too strong and/or that the sources of interference are angularly located in low sidelobe regions and are thus adequately filtered out by the beamforming operation. The next section develops a modification of the algorithm for strong interference scenarios.

B. Algorithmic Summary of 3D-BDMUSIC with $M \times 3$ Butler Matrix Beamforming

The algorithmic summary of the 3D-BDMUSIC with $M \times 3$ Butler matrix beamforming is as follows.

1) Form 3×1 beamspace snapshot vectors: $\boldsymbol{x}_B(n) = \boldsymbol{W}_B^H \boldsymbol{x}(n)$, $n = 1, \cdots, N$.

2) Construct 3×3 beamspace correlation matrix: $\hat{\boldsymbol{R}}_{bb} = (1/N) \sum_{n=0}^{N-1} \boldsymbol{x}_B(n) \boldsymbol{x}_B^H(n)$.

3) Compute $\boldsymbol{v} = [v_1, v_2, v_3]^T$ as EVEC of Re $\{\hat{\boldsymbol{R}}_{bb}\}$ associated with "smallest" EV.

4) Construct quadratic equation $e_*(z) = e_0 + e_1 z + e_0^* z^2$, where

$$e_0 = e^{j\pi u_c}\{v_1 e^{j(\pi/M)} - v_2 + v_3 e^{-j(\pi/M)}\};$$

$$e_1 = -2(v_1 + v_3)\cos\left(\frac{\pi}{M}\right) + 2v_2 \cos\left(\frac{2\pi}{M}\right).$$

5) Estimate $z_1 = e^{j\pi u_1}$ and $z_2 = e^{j\pi u_2}$ as the two roots of $e_*(z)$.

Step 1: The $M \times 3$ Butler matrix $\boldsymbol{W}_B$, defined in (2.2), performs a transformation from M-dimensional element space to 3-D beamspace.

Step 2: $\hat{\boldsymbol{R}}_{bb}$ is, in general, a complex-valued 3×3 matrix. The number of snapshots may be as small as one, i.e., $N = 1$, as in the case of monopulse radar.

Step 3: The following two properties of the $M \times 3$ Butler matrix beamformer are invoked in this step:

$$\boldsymbol{W}_B^H \boldsymbol{W}_B = \boldsymbol{I}_3 \tag{3.6}$$

$$\tilde{\boldsymbol{I}}_M \boldsymbol{W}_B = \boldsymbol{W}_B^*. \tag{3.7}$$

The first property is a mathematical statement that the columns of $\boldsymbol{W}_B$ are mutually orthonormal. Since it is assumed that the element space noise covariance matrix is a scalar multiple of $\boldsymbol{I}_M$, it follows that the beamspace space noise covariance matrix is a scalar multiple of $\boldsymbol{I}_3$. As a consequence, $\boldsymbol{v}$ is computed via a standard eigenvalue decomposition (EVD) as opposed to a generalized EVD. This simplifies the algorithm somewhat but will actually be more critical in the case of multifrequency operation to be discussed later.

The second property of $\boldsymbol{W}_B$, described by (3.7), is no more than a mathematical statement that each of the columns of $\boldsymbol{W}_B$ is conjugate centrosymmetric. As a consequence, the 3×1 beamspace manifold vector

$$\boldsymbol{b}(u) = \boldsymbol{W}_B^H \boldsymbol{a}(u; M) \tag{3.8}$$

is a real-valued vector for all u. This claim is substantiated by the following sequence of manipulations:

$$\boldsymbol{b}(u) = \boldsymbol{W}_B^H \boldsymbol{a}(u; M) = \boldsymbol{W}_B^H \tilde{\boldsymbol{I}}_M \tilde{\boldsymbol{I}}_M \boldsymbol{a}(u; M)$$
$$= \boldsymbol{W}_B^T \boldsymbol{a}^*(u; M) = \boldsymbol{b}^*(u) \tag{3.9}$$

where we have used the "trick" $\tilde{\boldsymbol{I}}_M \tilde{\boldsymbol{I}}_M = \boldsymbol{I}_M$. The fact that $\boldsymbol{b}(u)$ is a real-valued vector yields two advantageous features of operating in the beamspace domain defined by the beamspace transformation matrix $\boldsymbol{W}_B$. First, the EVD required is that of a real-valued 3×3 matrix, as opposed to a complex one. This provides a modest savings in computation. More importantly, though, it produces the same effect as a single forward–backward average in element space with much less computation and storage requirements. The effect of taking the real part of $\hat{\boldsymbol{R}}_{bb}$ is most clearly explained by considering the case of a single snapshot ($N = 1$), no noise, and no interference. In this case, $\hat{\boldsymbol{R}}_{bb}$ is of rank one and may be expressed as $\boldsymbol{B}\hat{\boldsymbol{R}}_{ss}\boldsymbol{B}^T$, where $\boldsymbol{B} = [\boldsymbol{b}(u_1) \vdots \boldsymbol{b}(u_2)]$ and

$$\hat{\boldsymbol{R}}_{ss} = \begin{bmatrix} A_1^2(n) & A_1(n)\,A_2(n)\,e^{-j\Delta\Psi(n)} \\ A_1(n)\,A_2(n)\,e^{j\Delta\Psi(n)} & A_2^2(n) \end{bmatrix} \tag{3.10}$$

$\Delta\Psi(n) = \phi_2(n) - \phi_1(n)$ is the phase difference between the two signals occurring at the center of the array aperture. Since $\boldsymbol{B}$ is a real-valued 3×2 matrix, Re $\{\hat{\boldsymbol{R}}_{bb}\} = \boldsymbol{B}$ Re $\{\hat{\boldsymbol{R}}_{ss}\}\boldsymbol{B}^T$ where

$$\text{Re}\,\{\hat{\boldsymbol{R}}_{ss}\} = \begin{bmatrix} A_1^2(n) & A_1(n)\,A_2(n)\cos(\Delta\Psi(n)) \\ A_1(n)\,A_2(n)\cos(\Delta\Psi(n)) & A_2^2(n) \end{bmatrix}. \tag{3.11}$$

It is evident that as long as $\Delta\Psi(n)$ is not equal to either $0°$ or $180°$, Re $\{\hat{\boldsymbol{R}}_{ss}\}$ is of rank two. Hence, Re $\{\hat{\boldsymbol{R}}_{bb}\} = \boldsymbol{B}$ Re $\{\hat{\boldsymbol{R}}_{ss}\}\boldsymbol{B}^T$ is of rank two. Under these conditions, i.e., single snapshot and no noise or interference, the smallest EV of Re $\{\hat{\boldsymbol{R}}_{bb}\}$ is zero and the corresponding EVEC is orthogonal to both $\boldsymbol{b}(u_1)$ and $\boldsymbol{b}(u_2)$ individually, i.e., $\boldsymbol{v}^T\boldsymbol{b}(u_i) = 0$, $i = 1, 2$. The anomalies occurring with either $\Delta\Psi(n) = 0°$ or $\Delta\Psi(n) = 180°$ will be discussed and dealt with at a later point.

Step 4: This step invokes another very important property of the $M \times 3$ Butler matrix beamformer described by (3.3). That is, the respective three beams associated with each of the three columns of $\boldsymbol{W}_B$ have $M - 3$ nulls in common [10], [12]. This is demonstrated in Fig. 1(a) for the case of an $M = 21$ element array and a center pointing angle of $u_c = 0$. Recall that $w_{BL}(z)$, $w_{BC}(z)$, and $w_{BR}(z)$ denote the $(M - 1)$th order polynomials associated with the first, second, and third columns of $\boldsymbol{W}_B$, respectively. Translated, this observation dictates that these three polynomials have $M - 3$ roots in common. The $M - 3$ common roots are located on the unit cicle at $z_m = \exp[j\pi(u_c + (2m/M)]$, $m = 2, \cdots, M - 2$. Let $c_B(z)$ denote the polynomial of order $M - 3$ having these $M - 3$ roots for which the coefficients exhibit conjugate centrosymmetry. (For n roots on the unit circle, it is always possible to find a corresponding polynomial of order n whose coefficients exhibit conjugate centrosymmetry.) It follows that

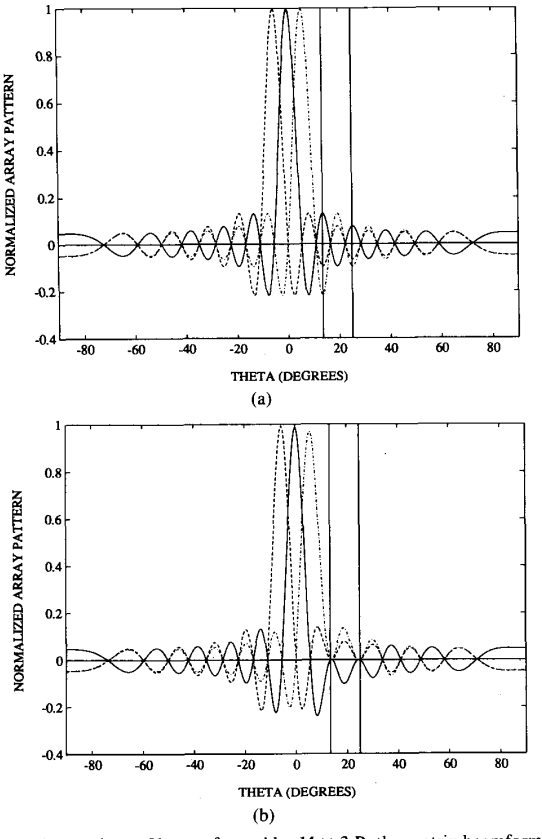

Fig. 1. Comparison of beams formed by $M \times 3$ Butler matrix beamformer with beams formed by $M \times 3$ interference cancellation matrix beamformer (ICMBF). $M = 21$ elements. Center pointing angle: $\theta_c = 0°$. Interference directions: $\theta_{I1} = 13.5°$ and $\theta_{I2} = 25°$. (a) Butler matrix beamforming. (b) Interference cancellation matrix beamforming.

$$w_{BL}(z) = c_B(z)\,q_{BL}(z); \qquad w_{BC}(z) = c_B(z)\,q_{BC}(z)$$
$$w_{BR}(z) = c_B(z)\,q_{BR}(z) \tag{3.12}$$

where $q_{BL}(z)$, $q_{BC}(z)$, and $q_{BR}(z)$ denote polynomials of order 2. The polynomial products in (3.12) give rise to the following convolutional relationships among the respective sequences:

$$\{w_{BL}\} = \{c_B\} * \{q_{BL}\}; \qquad \{w_{BC}\} = \{c_B\} * \{q_{BC}\}$$
$$\{w_{BR}\} = \{c_B\} * \{q_{BR}\}. \tag{3.13}$$

In turn, (3.12) gives rise to the following factorization of $\boldsymbol{W}_B$:

$$\boldsymbol{W}_B = \boldsymbol{C}_B\boldsymbol{Q}_B \tag{3.14}$$

where $\boldsymbol{C}_B$ is the $M \times 3$ banded, Toeplitz matrix

$$\boldsymbol{C}_B = \begin{bmatrix} c_B & 0 & 0 \\ 0 & c_B & 0 \\ 0 & 0 & c_B \end{bmatrix} \tag{3.15}$$

and $\boldsymbol{Q}_B$ is the 3×3 matrix

$$\boldsymbol{Q}_B = [\boldsymbol{q}_{\mathrm{BL}} \vdots \boldsymbol{q}_{\mathrm{BC}} \vdots \boldsymbol{q}_{\mathrm{BR}}]. \tag{3.16}$$

The 3-D beamspace domain version of MUSIC, 3D-BDMUSIC, prescribes that u_1 and u_2 be estimated as the two values of u for which $\boldsymbol{b}(u)$ is orthogonal to the 1-D subspace spanned by $\boldsymbol{v}$, the "smallest" EVEC of Re $\{\hat{\boldsymbol{R}}_{bb}\}$. The matrix factorization in (3.14) allows for an alternative formulation of this step in terms of finding the roots of a quadratic equation. This reformulation is suggested by the following sequence of manipulations:

$$\begin{aligned}\boldsymbol{v}^T\boldsymbol{b}(u_i) &= \boldsymbol{v}^T\boldsymbol{W}_B^H\boldsymbol{a}(u_i;\, M) = \boldsymbol{v}^T\boldsymbol{Q}_B^H\boldsymbol{C}_B^H\boldsymbol{a}(u_i;\, M)\\ &= (\boldsymbol{c}_B^H\boldsymbol{a}(u_i;\, M-2))(\boldsymbol{Q}_B\boldsymbol{v})^H\boldsymbol{a}(u_i;\, 3) = 0\\ &\qquad i = 1, 2\end{aligned} \tag{3.17}$$

where we have exploited the banded, Toeplitz structure of $\boldsymbol{C}_B$ and the Vandermonde structure of $\boldsymbol{a}(u;\, M)$. Since $\boldsymbol{c}_B^H\boldsymbol{a}(u_i;\, M-2)$ is a scalar, for $i = 1, 2$, (3.16) implies $(\boldsymbol{Q}_B\boldsymbol{v})^H\boldsymbol{a}(u_i;\, 3) = 0$, $i = 1, 2$. Let

$$\boldsymbol{e} = \boldsymbol{Q}_B\boldsymbol{v}. \tag{3.18}$$

It follows that $\hat{z}_i = e^{j\pi u_i}$, $i = 1, 2$, may be estimated as the two roots of $e_*(z)$, the second-order polynomial associated with $\boldsymbol{e}^* = \boldsymbol{Q}_B^*\boldsymbol{v}$.

Step 5: Formulation of the quadratic equation $e_*(z)$ requires the determination of $\boldsymbol{Q}_B$. To this end, note that the two roots of $w_{\mathrm{BL}}(z)$ which are not roots of $c_B(z)$ are $z = e^{j\pi u_c}$ and $z = \exp[j\pi(u_c + (2/M))]$. Hence,

$$\begin{aligned}q_{\mathrm{BL}}(z) &= \exp\left[-j\pi\left(u_c + \frac{1}{M}\right)\right](z - e^{j\pi u_c})\\ &\quad\cdot\left(z - \exp\left[j\pi\left(u_c + \frac{2}{M}\right)\right]\right)\\ &= \exp\left[j\pi\left(u_c + \frac{1}{M}\right)\right] - 2\cos\left(\frac{\pi}{M}\right)z\\ &\quad + \exp\left[-j\pi\left(u_c + \frac{1}{M}\right)\right]z^2.\end{aligned} \tag{3.19}$$

Similarly, the two roots of $w_{\mathrm{BC}}(z)$ which are not roots of $c_B(z)$ are $z = \exp[j\pi(u_c + (2/M))]$ and $z = \exp[j\pi(u_c - (2/M))]$. Hence,

$$\begin{aligned}q_{\mathrm{BC}}(z) &= -e^{-j\pi u_c}\left(z - \exp\left[j\pi\left(u_c + \frac{2}{M}\right)\right]\right)\\ &\quad\cdot\left(z - \exp\left[j\pi\left(u_c - \frac{2}{M}\right)\right]\right)\\ &= -e^{j\pi u_c} + 2\cos\left(\frac{2\pi}{M}\right)z - e^{-j\pi u_c}z^2.\end{aligned} \tag{3.20}$$

Finally, the two roots of $w_{\mathrm{BR}}(z)$ which are not roots of $c_B(z)$ are $z = e^{j\pi u_c}$ and $z = \exp[j\pi(u_c - (2/M))]$. Hence,

$$\begin{aligned}q_{\mathrm{BR}}(z) &= \exp\left[-j\pi\left(u_c - \frac{1}{M}\right)\right](z - e^{j\pi u_c})\\ &\quad\cdot\left(z - \exp\left[j\pi\left(u_c - \frac{2}{M}\right)\right]\right)\\ &= \exp\left[j\pi\left(u_c - \frac{1}{M}\right)\right] - 2\cos\left(\frac{\pi}{M}\right)z\\ &\quad + \exp\left[-j\pi\left(u_c - \frac{1}{M}\right)\right]z^2.\end{aligned} \tag{3.21}$$

Consider $\boldsymbol{q}_{\mathrm{BL}}$, $\boldsymbol{q}_{\mathrm{BC}}$, and $\boldsymbol{q}_{\mathrm{BR}}$, the 3×1 coefficient vectors associated with $q_{\mathrm{BL}}(z)$, $q_{\mathrm{BC}}(z)$, and $q_{\mathrm{BR}}(z)$, respectively. From (3.19)–(3.21),

$$\begin{aligned}\boldsymbol{q}_{\mathrm{BL}} &= \begin{bmatrix} \exp\left[j\pi\left(u_c + \frac{1}{M}\right)\right] \\ -2\cos\left(\frac{\pi}{M}\right) \\ \exp\left[-j\pi\left(u_c + \frac{1}{M}\right)\right] \end{bmatrix}\\ \boldsymbol{q}_{\mathrm{BC}} &= \begin{bmatrix} -e^{j\pi u_c} \\ 2\cos\left(\frac{2\pi}{M}\right) \\ -e^{-j\pi u_c} \end{bmatrix}\\ \boldsymbol{q}_{\mathrm{BR}} &= \begin{bmatrix} \exp\left[j\pi\left(u_c - \frac{1}{M}\right)\right] \\ -2\cos\left(\frac{\pi}{M}\right) \\ \exp\left[-j\pi\left(u_c - \frac{1}{M}\right)\right] \end{bmatrix}.\end{aligned} \tag{3.22}$$

Note that each of the columns of $\boldsymbol{Q}_B$, i.e., each of the vectors listed in (3.22), is conjugate centrosymmetric such that $\tilde{\boldsymbol{I}}_3\boldsymbol{Q}_B = \boldsymbol{Q}_B^*$. As $\boldsymbol{v}$ is real, it follows that $\boldsymbol{e} = \boldsymbol{Q}_B\boldsymbol{v}$ is conjugate centrosymmetric as well. Upon substitution, we arrive at the following expressions for the components of $\boldsymbol{e} = \boldsymbol{Q}_B\boldsymbol{v}$:

$$\begin{aligned}e_0 &= e^{j\pi u_c}\{v_1e^{j(\pi/M)} - v_2 + v_3e^{-j(\pi/M)}\} = e_2^*;\\ e_1 &= -2(v_1 + v_3)\cos\left(\frac{\pi}{M}\right) + 2v_2\cos\left(\frac{2\pi}{M}\right).\end{aligned} \tag{3.23}$$

The final step in the algorithm then is to estimate $z_1 = e^{j\pi u_1}$ and $z_2 = e^{j\pi u_2}$ as the two roots of $e_*(z) = e_0 + e_1z + e_0^*z^2$.

It is apparent that the ability to factor the $M \times 3$ Butler matrix beamformer $\boldsymbol{W}_B$ as $\boldsymbol{C}_B\boldsymbol{Q}_B$, where $\boldsymbol{C}_B$ is an $M \times 3$ banded-Toeplitz matrix, is critical to the computational simplicity of 3D-BDMUSIC. This property facilitates the formulation of the final step in terms of the solution of a quadratic equation, as opposed to a nonlinear search over

the beamspace manifold. As a consequence, this structure will be imposed in the construction of an $M \times 3$ matrix beamformer suitable for operation in the presence of strong interferers environment. An appropriate procedure is developed in the next section.

IV. MVDR-Based Construction of the Interference Cancellation Matrix Beamformer

In the case of strong interference, it is necessary to modify the locations of the nulls of each of the three beams achieved with $M \times 3$ Butler matrix beamforming, i.e., formed by each of the three columns of $\boldsymbol{W}_B$. In order to nullify the effect of the jammers, each beam ideally exhibits a null in the direction of each and every point-like interferer. If an interferer is spatially distributed or continuous, each beam should exhibit a suitable number of nulls in the angular vicinity of the interfering source. Let u_{Ik}, $k = 1, \cdots, K$, denote the directions in which nulls are to be formed. We will not here concern ourselves with the estimation of the locations of the interferers. We will simply assume that these null locations have been judiciously determined by employing a high quality, parametric spatial spectral estimator such as ESPRIT [19], [20], MUSIC [17], IQML [18], etc., during a passive listening period in which the radar is not transmitting. Let $\boldsymbol{W}_I$ denote the $M \times 3$ matrix beamformer to be employed in the case of strong interference. As the case with $\boldsymbol{W}_B$, the first, second, and third columns of $\boldsymbol{W}_I$ denote the weight vectors for forming the left, center, and right adaptive beams. Correspondingly,

$$\boldsymbol{W}_I = [\boldsymbol{w}_{\mathrm{IL}} \vdots \boldsymbol{w}_{\mathrm{IC}} \vdots \boldsymbol{w}_{\mathrm{IR}}]. \tag{4.1}$$

The null constraints to be satisfied may be mathematically expressed as

$$\boldsymbol{W}_I^H \boldsymbol{a}(u_{Ik}; M) = \begin{bmatrix} 0 \\ 0 \\ 0 \end{bmatrix} \qquad k = 1, 2, \cdots, K. \tag{4.2}$$

In order to maintain the computational simplicity of 3D-BDMUSIC achieved with the $M \times 3$ Butler matrix beamformer, we will further impose that $\boldsymbol{W}_I$ be constructed in such a manner that it may be factored as

$$\boldsymbol{W}_I = \boldsymbol{C}_I \boldsymbol{Q}_I \tag{4.3}$$

where $\boldsymbol{C}_I$ is an $M \times 3$ banded, Toeplitz matrix of the form

$$\boldsymbol{C}_I = \begin{bmatrix} \boldsymbol{c}_I & 0 & 0 \\ 0 & \boldsymbol{c}_I & 0 \\ 0 & 0 & \boldsymbol{c}_I \end{bmatrix} \tag{4.4}$$

and $\boldsymbol{Q}_I$ is a 3×3 matrix, the columns of which are denoted as

$$\boldsymbol{Q}_I = [\boldsymbol{q}_{\mathrm{IL}} \vdots \boldsymbol{q}_{\mathrm{IC}} \vdots \boldsymbol{q}_{\mathrm{IR}}]. \tag{4.5}$$

$\boldsymbol{c}_I$ is an $(M - 2) \times 1$ vector; the $M - 3$ roots of $\boldsymbol{c}_I(z)$ correspond to the $M - 3$ common nulls among the three beams. K of these $M - 3$ common roots correspond to the respective nulls formed in each of the interference directions u_{Ik}, $k = 1, \cdots, K$. The other $M - K - 3$ roots will be chosen so as to minimize some measure of the noise present at each of the three beamformer outputs.

In addition to the factorization in (4.3), we will also impose that the columns of $\boldsymbol{W}_I$ be mutually orthonormal and that each exhibit conjugate centrosymmetry. Mathematically, the two additional constraints on the structure of $\boldsymbol{W}_I$ are

$$\boldsymbol{W}_I^H \boldsymbol{W}_I = \boldsymbol{I}_3 \tag{4.6}$$

$$\tilde{\boldsymbol{I}}_M \boldsymbol{W}_I = \boldsymbol{W}_I^*. \tag{4.7}$$

The conjugate centrosymmetry constraint in (4.7) serves to constrain the 3×1 beamspace manifold vector $\boldsymbol{b}_I(u) = \boldsymbol{W}_I^H \boldsymbol{a}(u; M)$ to be real valued. In turn, this facilitates the effecting of a single forward–backward average in element space by simply taking the real part of the 3×3 beamspace correlation matrix. Correspondingly, it allows us to work with a real-valued matrix, as opposed to a complex one. Translated, the orthonormality constraint in (4.6) implies that the 3×3 beamspace noise correlation matrix is a scalar multiple of $\boldsymbol{I}_3$. This allows us to avoid a generalized EVD, and will be important in the case of multifrequency operation. With $\boldsymbol{W}_I$ satisfying (4.3), (4.6), and (4.7), the only changes to the 3D-BDMUSIC algorithm outlined previously is that $\boldsymbol{W}_I$ replaces $\boldsymbol{W}_B$ and that $\boldsymbol{e}$ in step 4 is computed as $\boldsymbol{e} = \boldsymbol{Q}_I \boldsymbol{v}$. A novel procedure for constructing $\boldsymbol{W}_I$, and $\boldsymbol{Q}_I$ as well, satisfying all of these conditions is now developed.

A. Construction of Center Beam

To facilitate a simple procedure for satisfying the constraint in (4.3) that the three beams have $M - 3$ nulls in common, the following approach is taken. The weight vector associated with the center beam, $\boldsymbol{w}_{\mathrm{IC}}$, is constructed first. $\boldsymbol{w}_{\mathrm{IL}}$ and $\boldsymbol{w}_{\mathrm{IR}}$ are then constructed based on $\boldsymbol{w}_{\mathrm{IC}}$. $\boldsymbol{w}_{\mathrm{IC}}$ is determined as that weight vector which minimizes the expected power of the noise present at the beamformer output subject to a number of null constraints and a unity gain constraint in the direction u_c. In addition to the K null constraints associated with the prescribed interference directions, two additional null constraints are imposed. Ultimately, these produce the two nulls of the center beam which are not members of the set of $M - 3$ nulls common to the three beams formed by the columns of $\boldsymbol{W}_I$. For a variety of reasons, we choose the positions of these two nulls to be the same as the locations of the two "uncommon" nulls associated with the center beam in the case of $M \times 3$ Butler matrix beamforming, $u = u_c - (2/M)$ and $u = u_c + (2/M)$. These are the locations of the first null on either side of the mainlobe of the beam formed with $\boldsymbol{w}_{\mathrm{BC}}$, the center column of $\boldsymbol{W}_B$. Under the assumption that none of the prescribed interference directions is within two beamwidths of the mainlobe of the

center beam, this serves to maintain the integrity of the mainlobe of the center beam relative to that achieved with $\boldsymbol{w}_{\mathrm{BC}}$. As we shall see, this also yields significant benefits in the case of multifrequency operation. If one of the interferers is located in this region, an additional beam must be formed and 3D-BDMUSIC applied in a four-dimensional beamspace. The 3D-BDMUSIC described previously generalizes for higher dimensional beamspaces. However, we herein consider only the case in which each of the interferers is located at least two beamwidths away from the pointing angle of the center beam.

We will shortly describe several alternative methods for constructing $\boldsymbol{w}_{\mathrm{IC}}$ as the solution to the constrained optimization problem described above. Assume for the moment, however, that $\boldsymbol{w}_{\mathrm{IC}}$ has been generated which satisfies the above specifications. Given that the two corresponding "uncommon" nulls are located at $u = u_c - (2/M)$ and $u = u_c + (2/M)$, this approach automatically specifies that the $(M-3)$th order "common roots" polynomial $c_I(z)$ is given by the polynomial ratio

$$c_I(z) = \frac{w_{\mathrm{IC}}(z)}{q_{\mathrm{IC}}(z)} \tag{4.8}$$

where $q_{\mathrm{IC}}(z) = q_{\mathrm{BC}}(z)$ given by (3.19). Accordingly, the length $M-2$ sequence $\{c_I\}$ may be computed by simply deconvolving the length 3 sequence $\{q_{\mathrm{IC}}\} = \{q_{\mathrm{BC}}\}$ out of the length M sequence $\{w_{\mathrm{IC}}\}$. This approach then dictates that each of the two sequences $\{w_{\mathrm{IL}}\}$ and $\{w_{\mathrm{IR}}\}$ must be the linear convolution of $\{c_I\}$ with a sequence of length 3, i.e.,

$$\{w_{\mathrm{IL}}\} = \{c_I\} * \{q_{\mathrm{IL}}\} \quad \text{and } \{w_{\mathrm{IR}}\} = \{c_I\} * \{q_{\mathrm{IR}}\}. \tag{4.9}$$

In this mode of operation, the final step in the construction of $\boldsymbol{W}_I$ is to determine the length three sequences $\{q_{\mathrm{IL}}\}$ and $\{q_{\mathrm{IR}}\}$ under the restriction that $\boldsymbol{W}_I$ exhibit the properties described by (4.6) and (4.7). These two restrictions do not uniquely specify $\{q_{\mathrm{IL}}\}$ and $\{q_{\mathrm{IR}}\}$. Final selection of $\{q_{\mathrm{IL}}\}$ and $\{q_{\mathrm{IR}}\}$ will be dictated by some constraints on the shape of the respective beams formed by $\boldsymbol{w}_{\mathrm{IL}}$ and $\boldsymbol{w}_{\mathrm{IR}}$. A number of alternatives will be considered.

In accordance with the above discussion, $\boldsymbol{w}_{\mathrm{IC}}$ is the solution to the following constrained optimization problem:

$$\begin{aligned} &\underset{\boldsymbol{w}_{\mathrm{IC}}}{\text{Minimize}}\ E\{|\boldsymbol{w}_{\mathrm{IC}}^H \boldsymbol{n}(n)|^2\} = \sigma_n^2 \|\boldsymbol{w}_{\mathrm{IC}}\|^2 \\ &\text{subject to:} \quad \boldsymbol{A}_{\mathrm{IC}}^H \boldsymbol{w}_{\mathrm{IC}} = \delta \end{aligned} \tag{4.10}$$

where σ_n^2 is the variance of the i.i.d. receiver generated noise at each element, $\boldsymbol{A}_{\mathrm{IC}}$ is the $M \times (K+3)$ matrix

$$\boldsymbol{A}_{\mathrm{IC}} = \left[\boldsymbol{a}(u_c; M) \vdots \boldsymbol{a}\left(u_c + \frac{2}{M}; M\right) \vdots \boldsymbol{a}\left(u_c - \frac{2}{M}; M\right) \vdots \boldsymbol{a}(u_{I1}; M) \vdots \cdots \vdots \boldsymbol{a}(u_{\mathrm{IK}}; M)\right] \tag{4.11}$$

and $\delta = [1, 0, 0, \cdots, 0]^T$, a $(K+3) \times 1$ vector. The solution is simply the minimum norm solution to the constraint equation in (4.10)

$$\boldsymbol{w}_{\mathrm{IC}} = \boldsymbol{A}_{\mathrm{IC}}(\boldsymbol{A}_{\mathrm{IC}}^H \boldsymbol{A}_{\mathrm{IC}})^{-1}\delta. \tag{4.12}$$

As a consequence of the conjugate centrosymmetry of each of the columns of $\boldsymbol{A}_{\mathrm{IC}}$, it is easy to show that the solution for $\boldsymbol{w}_{\mathrm{IC}}$ described by (4.12) is conjugate centrosymmetric.

We briefly describe several alternative methods for computing the solution $\boldsymbol{w}_{\mathrm{IC}}$ to the optimization problem in (4.10) which offer certain advantages over direct computation according to (4.12). The first method is a two step procedure based on Gram–Schmidt orthogonalization. In the first step, the Gram–Schmidt procedure is used to find an orthonormal basis, denoted $\{\boldsymbol{e}_1, \boldsymbol{e}_2, \cdots, \boldsymbol{e}_{K+2}\}$, for the $(K+2)$-dimensional subspace spanned by the set of vectors $\{\boldsymbol{a}(u_c + (2/M); M), \boldsymbol{a}(u_c - (2/M); M), \boldsymbol{a}(u_{I1}; M), \cdots, \boldsymbol{a}(u_{\mathrm{IK}}; M)\}$. Once the orthonormal basis is determined, $\boldsymbol{w}_{\mathrm{IC}}$ is determined, to within a scalar multiple, by subtracting from $\boldsymbol{a}(u_c; M)$ its projection onto this $(K+2)$-dimensional space, i.e., $\boldsymbol{w}_{\mathrm{IC}} = \boldsymbol{a}(u_c; M) - \sum_{i=1}^{K+2} \{\boldsymbol{e}_i^H \boldsymbol{a}(u_c; M)\}\boldsymbol{e}_i$.

Computation of $\boldsymbol{w}_{\mathrm{IC}}$ according to either (4.12) or by the Gram–Schmidt based procedure sketched above explicitly requires estimates of the interference directions u_{IK}, $k = 1, \cdots, K$. Alternatively, MUSIC [17] may be employed to estimate an orthonormal basis for the K-dimensional subspace range $\{\boldsymbol{a}(u_{I1}; M), \cdots, \boldsymbol{a}(u_{\mathrm{IK}}; M)\}$ as the K principal eigenvectors of $\hat{\boldsymbol{R}}_{xx} = 1/N \sum_{n=1}^{N} \boldsymbol{x}(n)\boldsymbol{x}^H(n)$, the sample correlation matrix formed during a period in which the radar array is passively listening. A simple two step Gram–Schmidt procedure may then be implemented to expand to an orthonormal basis of $K+2$ vectors encompassing the space spanned by $\boldsymbol{a}(u_c + (2/M); M)$ and $\boldsymbol{a}(u_c - (2/M); M)$ as well. Note that this Gram–Schmidt based procedure will yield a $\boldsymbol{w}_{\mathrm{IC}}$ exhibiting conjugate centrosymmetry if the principal eigenvectors are each conjugate centrosymmetric. This will be the case if we use the principal eigenvectors of $\hat{\boldsymbol{R}}_{\mathrm{FB}} = 1/2\{\hat{\boldsymbol{R}}_{xx} + \tilde{\boldsymbol{I}}_M \hat{\boldsymbol{R}}_{xx}^* \tilde{\boldsymbol{I}}_M\}$, the forward–backward averaged sample correlation matrix over the entire aperture, as opposed to those of $\hat{\boldsymbol{R}}_{xx}$ itself [10], [12].

Along these lines, the eigenvalue decomposition (EVD) required by MUSIC may be avoided if we forego "hard nulls" in the direction of the interferers and compute $\boldsymbol{w}_{\mathrm{IC}}$ according to a slight modification of the classical minimum variance distortionless response (MVDR) criterion. To this end, consider the constrained optimization problem

$$\begin{aligned} &\underset{\boldsymbol{w}_{\mathrm{IC}}}{\text{Minimize}}\ E\{|\boldsymbol{w}_{\mathrm{IC}}^H \boldsymbol{x}(n)|^2\} = \boldsymbol{w}_{\mathrm{IC}}^H \hat{\boldsymbol{R}}_{xx} \boldsymbol{w}_{\mathrm{IC}} \\ &\text{subject to:} \quad \boldsymbol{W}_B^H \boldsymbol{w}_{\mathrm{IC}} = \boldsymbol{f} \\ &\qquad\qquad \tilde{\boldsymbol{I}}_M \boldsymbol{w}_{\mathrm{IC}} = \boldsymbol{w}_{\mathrm{IC}}^*. \end{aligned} \tag{4.13}$$

Here $\boldsymbol{f} = [0, 1, 0]^T$ such that $\boldsymbol{w}_{\mathrm{IC}}$ is chosen to minimize the expected power at the beamformer output subject to a unity gain constraint in the direction $u = u_c$, and a null constraint in each of the directions $u = u_c - (2/M)$ and

$u = u_c + (2/M)$ to facilitate simple construction of the left and right beams. Using the method of Lagrange multipliers, it is easily shown that the solution is

$$\boldsymbol{w}_{\mathrm{IC}} = \hat{\boldsymbol{R}}_{\mathrm{FB}}^{-1}\boldsymbol{W}_B(\boldsymbol{W}_B^H\hat{\boldsymbol{R}}_{\mathrm{FB}}^{-1}\boldsymbol{W}_B)^{-1}\boldsymbol{f} \tag{4.14}$$

where $\hat{\boldsymbol{R}}_{\mathrm{FB}} = 1/2\{\hat{\boldsymbol{R}}_{xx} + \tilde{\boldsymbol{I}}_M\hat{\boldsymbol{R}}_{xx}^*\tilde{\boldsymbol{I}}_M\}$ as defined above. Note that since $\tilde{\boldsymbol{I}}_M\hat{\boldsymbol{R}}_{\mathrm{FB}}\tilde{\boldsymbol{I}}_M = \hat{\boldsymbol{R}}_{\mathrm{FB}}^*$, it easy to verify that $\tilde{\boldsymbol{I}}_M\hat{\boldsymbol{R}}_{\mathrm{FB}}^{-1}\tilde{\boldsymbol{I}}_M = \hat{\boldsymbol{R}}_{\mathrm{FB}}^{-1*}$ as well. Based on this result and the fact that the columns of $\boldsymbol{W}_B$ are conjugate centrosymmetric, it is easy to show that $\boldsymbol{w}_{\mathrm{IC}}$ computed according to (4.14) is conjugate centrosymmetric as desired. Note that this method requires an inverse of $\hat{\boldsymbol{R}}_{\mathrm{FB}}$ as opposed to an EVD of such as required by the MUSIC based procedure described above. However, this procedure may not yield nulls of significant depth to combat strong interferers.

An alternative procedure for computing $\boldsymbol{w}_{\mathrm{IC}}$ requires only the coefficients of the so-called interference polynomial

$$\begin{aligned} i(z) &= \alpha_I(z - e^{j\pi u_{I1}})(z - e^{j\pi u_{I2}}) \cdots (z - e^{j\pi u_{IK}}) \\ &= i_0 + i_1 z + i_2 z^2 + \cdots + i_K z^K \end{aligned} \tag{4.15}$$

where α_I is that scalar which makes the sequence $\{\boldsymbol{i}\}$ conjugate centrosymmetric. That is, in the alternative procedure to be described it is not necessary to determine the roots of $i(z)$. An estimate of the coefficient sequence $\{\boldsymbol{i}\}$ may be extracted from either the IQML [18], TLS-ESPRIT [19], or PRO-ESPRIT [20] algorithms without the need for rooting [18]. The second step in this procedure is to convolve the length $K + 1$ sequence $\{\boldsymbol{i}\}$ with the length 3 sequence $\{\boldsymbol{q}_{\mathrm{BC}}\}$, defined by (3.20), yielding a length $K + 3$ sequence denoted $\{\boldsymbol{i}_c\}$, i.e., $\{\boldsymbol{i}_c\} = \{\boldsymbol{i}\} * \{\boldsymbol{q}_{\mathrm{BC}}\}$. Note that the convolution of two conjugate centrosymmetric sequences yields a conjugate centrosymmetric sequence. $\{\boldsymbol{w}_{\mathrm{IC}}\}$ is then computed as the convolution of $\{\boldsymbol{i}_c\}$ with some sequence of length $M - K - 2$, denoted arbitrarily as $\{\boldsymbol{d}_c\}$. In matrix formulation

$$\boldsymbol{w}_{\mathrm{IC}} = \boldsymbol{I}_c\boldsymbol{d}_c \qquad \text{where: } \boldsymbol{I}_c = \begin{bmatrix} \boldsymbol{i}_c & 0 & 0 \\ 0 & \boldsymbol{i}_c & 0 \\ 0 & 0 & \ddots\ 0 \\ \vdots & \vdots & \vdots \\ 0 & 0 & \boldsymbol{i}_c \end{bmatrix}. \tag{4.16}$$

Note that $\boldsymbol{I}_c$ is an $M \times (M - K - 2)$ banded Toeplitz matrix.

Construction of $\boldsymbol{w}_{\mathrm{IC}}$ according to (4.16) guarantees that the $(M - 1)$th order polynomial $w_{\mathrm{IC}}(z)$ has roots at $z_{\mathrm{Ik}} = e^{j\pi u_{\mathrm{Ik}}}$, $k = 1, \cdots, K$, and at $z_L = \exp[j\pi(u_c - (2/M))]$ and $z_R = \exp[j\pi(u_c + (2/M))]$. Correspondingly, the beam produced by $\boldsymbol{w}_{\mathrm{IC}}$ will exhibit nulls at each of the interference directions u_{Ik}, $k = 1, \cdots, K$, and at $u_L = u_c - (2/M)$ and $u_R = u_c + (2/M)$ as required. Determination of the $(M - K - 2) \times 1$ vector $\boldsymbol{d}_c$ is dictated by compliance with the constrained optimization problem in (4.10) which, upon substitution of (4.16), may be alternatively expressed as

$$\begin{aligned} &\underset{\boldsymbol{d}_c}{\text{Minimize}}\ \|\boldsymbol{w}_{\mathrm{IC}}\|^2 = \boldsymbol{d}_c^H\boldsymbol{I}_c^H\boldsymbol{I}_c\,\boldsymbol{d}_c \\ &\text{subject to:}\quad \boldsymbol{w}_{\mathrm{IC}}^H\boldsymbol{a}(u_c; M) = \boldsymbol{d}_c^H\boldsymbol{I}_c^H\boldsymbol{a}(u_c; M) = 1. \end{aligned} \tag{4.17}$$

The null constraints are already incorporated in the construction of $\boldsymbol{w}_{\mathrm{IC}}$ according to (4.16). Solving (4.17) via the method of Lagrange leads to the result that $\boldsymbol{d}_c$ be determined as the solution to the $(M - K - 2) \times (M - K - 2)$ system of equations

$$\boldsymbol{I}_c^H\boldsymbol{I}_c\,\boldsymbol{d}_c = \lambda_{\mathrm{IC}}\boldsymbol{I}_c^H\boldsymbol{a}(u_c; M) \tag{4.18}$$

where λ_{IC} is a Lagrange multiplier. Of course, the solution is simply $\boldsymbol{d}_c = \lambda_{\mathrm{IC}}(\boldsymbol{I}_c^H\boldsymbol{I}_c)^{-1}\boldsymbol{I}_c^H\boldsymbol{a}(u_c; M)$. Complying with the unity gain constraint in (4.17) yields $\lambda_{\mathrm{IC}} = \{\boldsymbol{a}^H(u_c; M)\,\boldsymbol{P}_{I_c}\boldsymbol{a}(u_c; M)\}^{-1}$, where $\boldsymbol{P}_{I_c}$ is the projection operator onto range $\{\boldsymbol{I}_c\}$. Thus, λ_{IC} is observed to be real.

A number of important observations may be gleaned from (4.18). First, as a consequence of the banded, Toeplitz structure of $\boldsymbol{I}_c$, it follows that $\boldsymbol{I}_c^H\boldsymbol{I}_c$ is an $(M - K - 2) \times (M - K - 2)$ Toeplitz–Hermitian matrix. Hence, (4.18) may be efficiently solved via the Levinson–Durbin recursion. Note that the elements of the first column of $\boldsymbol{I}_c^H\boldsymbol{I}_c$ are simply the first $M - K - 2$ autocorrelation values for the sequence $\{\boldsymbol{i}_c\}$. Second, the solution $\boldsymbol{d}_c$ to (4.18) is conjugate centrosymmetric. Thus, computation of the solution to (4.18) via the Levinson–Durbin recursion may be terminated at iteration number $(M - K - 2)/2$, in the case of $M - K - 2$ even, or iteration number $(M - K - 1)/2$, in the case of $M - K - 2$ odd. Proof of the conjugate centrosymmetry of $\boldsymbol{d}_c$ is achieved by invoking the Toeplitz–Hermitian structure of $\boldsymbol{I}_c^H\boldsymbol{I}_c$, the conjugate centrosymmetry of $\boldsymbol{a}(u_c; M)$, and the fact that λ_{IC} is real. The proof is trivial and thus not included here. As a consequence, $\{\boldsymbol{w}_{\mathrm{IC}}\} = \{\boldsymbol{i}_c\} * \{\boldsymbol{d}_c\}$ is a conjugate centrosymmetric sequence and $\boldsymbol{w}_{\mathrm{IC}}$ is a conjugate centrosymmetric vector.

An important insight is provided by identifying $\boldsymbol{w}_{\mathrm{IC}} = \boldsymbol{I}_c\,\boldsymbol{d}_c$ in (4.18). With this substitution, (4.18) may be expressed as $\boldsymbol{I}_c^H\boldsymbol{w}_{\mathrm{IC}} = \lambda_{\mathrm{IC}}\boldsymbol{I}_c^H\boldsymbol{a}(u_c; M)$ from which we deduce that the solution is such that $\boldsymbol{w}_{\mathrm{IC}} \approx \boldsymbol{a}(u_c; M)$. In loose terms, $\boldsymbol{w}_{\mathrm{IC}}$ is attempting to emulate the classical beamformer $\boldsymbol{w}_{\mathrm{BC}} = \boldsymbol{a}(u_c; M)$ as best as possible under the given null constraints. We will invoke this observation shortly.

B. Construction of Left and Right Adaptive Beams

Once the solution $\boldsymbol{w}_{\mathrm{IC}}$ to (4.10) has been determined according to one of the five computational procedures described above, $\boldsymbol{c}_I$ is readily determined in accordance with (4.8). As discussed previously, the length $M - 2$ sequence $\{\boldsymbol{c}_I\}$ is computed by simply deconvolving the length 3 sequence $\{\boldsymbol{q}_{\mathrm{BC}}\}$, defined by (3.19), out of the length M sequence $\{\boldsymbol{w}_{\mathrm{IC}}\}$. Note that $\{\boldsymbol{w}_{\mathrm{IC}}\}$ and $\{\boldsymbol{q}_{\mathrm{BC}}\}$ are each conjugate centrosymmetric such that $\{\boldsymbol{c}_I\}$ is conjugate centrosymmetric as well. $\{\boldsymbol{w}_{\mathrm{IL}}\}$ and $\{\boldsymbol{w}_{\mathrm{IR}}\}$ are then each determined by convolving $\{\boldsymbol{c}_I\}$ with a sequence of

length 3, denoted $\{q_{IL}\}$ and $\{q_{IR}\}$, respectively, as described in (4.9). In matrix formulation

$$w_{IL} = C_I q_{IL}; \qquad w_{IR} = C_I q_{IR} \tag{4.19}$$

where C_I is the $M \times 3$ banded, Toeplitz matrix constructed from c_I according to (4.4). Note that it is guaranteed that each of the two respective beams formed with w_{IL} and w_{IR} exhibits a null in the direction of each and every interferer. It thus seems logical to determine q_{IL} and q_{IR} by using the two remaining degrees of freedom in each beam to suppress the noise at the corresponding beamformer output as best as possible subject to a unity gain constraint in some specified direction. In light of the desirable properties of the $M \times 3$ Butler matrix beamformer, we choose the pointing angles of the left and right beams to be $u_L = u_c - (2/M)$ and $u_R = u_c + (2/M)$, respectively.

With the assumption of i.i.d. receiver generated noise, this criterion leads to the following constrained optimization problem with respect to the left beam:

$$\underset{q_{IL}}{\text{Minimize}}\ w_{IL}^H w_{IL} = q_{IL}^H C_I^H C_I q_{IL}$$

$$\text{subject to:} \quad w_{IL}^H a\left(u_c - \frac{2}{M}; M\right) = q_{IL}^H C_I^H a\left(u_c - \frac{2}{M}; M\right) = 1. \tag{4.20}$$

Solving (4.20) via the method of Lagrange leads to the result that q_{IL} is determined as the solution to the 3×3 system of equations

$$C_I^H C_I q_{IL} = \lambda_{IL} C_I^H a\left(u_c - \frac{2}{M}; M\right) \tag{4.21}$$

where λ_{IL} is the Lagrange multiplier associated with the unity gain constraint in (4.20). Every comment made with respect to (4.18) can be made with respect to (4.21) with minor modification: $C_I^H C_I$ is a 3×3 Toeplitz–Hermitian matrix, the appropriate λ_{IL} is real valued, and q_{IL} which solves (4.21) exhibits conjugate centrosymmetry. Also, in loose terms, w_{IL} is attempting to emulate the classical beamformer $w_{BL} = a(u_c - (2/M); M)$ as best as possible under the constraints imposed. This is deduced by observing that the q_{IL} which solves (4.21) is the least square error solution to $C_I q_{IL} = \lambda_{IL} a(u_c - (2/M); M)$ and that $w_{IL} = C_I q_{IL}$.

A constrained optimization problem similar to (4.20) with q_{IL} replaced by q_{IR} and $u_c - (2/M)$ replaced by $u_c + (2/M)$ leads to the result that q_{IR} is determined as the solution to the 3×3 system of equations

$$C_I^H C_I q_{IR} = \lambda_{IR} C_I^H a\left(u_c + \frac{2}{M}; M\right). \tag{4.22}$$

Again, similar comments hold with the most important being that the q_{IR} which solves (4.22) exhibits conjugate centrosymmetry. Also, once again, it is apparent that $w_{IR} = C_I q_{IR}$ is attempting to emulate the classical beamformer $w_{BR} = a(u_c + (2/M); M)$ as best as possible under the constraints imposed.

Let $W_I = C_I Q_I$, where $Q_I = [q_{IL} \vdots q_{IC} \vdots q_{IR}]$ with q_{IL} and q_{IR} determined by solving (4.21) and (4.22), respectively, and $q_{IC} = q_{BC}$. Unfortunately, the three columns of W_I constructed in this fashion are *not*, in general, mutually orthogonal. Thus, in general, the beamspace noise realized with this $M \times 3$ matrix beamformer will be correlated from beamport to beamport, a condition we seek to avoid. Now, it is apparent from the discussion that in attempting to minimize the expected power of the noise present at each of the beamformers outputs, W_I is attempting to emulate W_B, the $M \times 3$ Butler matrix beamformer, as best as possible under the null constraints described by (4.2) and the constraint that the respective beams formed by w_{IL}, w_{IC}, and w_{IR} have $M - 3$ nulls in common. Incorporation of an orthonormality constraint on the columns of W_I into the above procedure for constructing W_I leads one to consider determining Q_I as the solution to the following constrained least square error (LSE) problem:

$$\underset{Q_I}{\text{Minimize}}\ \|W_B - W_I\|_F^2 = \|W_B - C_I Q_I\|_F^2$$

$$\text{subject to:} \quad W_I^H W_I = Q_I^H \{C_I^H C_I\} Q_I = I_3$$

$$\tilde{I}_3 W_I = \tilde{I}_3 \{C_I Q_I\} = \{C_I Q_I\}^* = W_I^*. \tag{4.23}$$

The solution to (4.23) will be evaluated under the assumption that C_I is determined in accordance with the procedure outlined previously. This dictates that $q_{IC} = q_{BC}$. To facilitate efficient computation of the solution to (4.23), Q_I is factored as $Q_I = QT_Q$ where Q is a 3×3 matrix computed via a Gram–Schmidt procedure such that the columns of $W_Q = C_I Q$ are orthonormal and conjugate centrosymmetric, and T_Q is a 3×3 orthogonal matrix. This enables us to reformulate the constrained optimization problem described by (4.23) as a Procrustes rotation problem [20] which is easily solved. The appropriate development is provided below.

The construction of Q may be accomplished by constructing an orthonormal basis for a 3-D Hilbert space with inner product defined by $\langle x, y \rangle = x^H C_I^H C_I y$. Let this basis be denoted q_L, q_C, and q_R. As the objective function in (4.23) dictates that $W_I = C_I Q_I$ be "close" to W_B in a Frobinius norm sense, it seems logical to employ the Gram–Schmidt procedure to construct q_L, q_C, and q_R using as an initial basis q_{BL}, q_{BC}, and q_{BR} defined in (3.21). As each of these vectors is conjugate centrosymmetric, this also serves to facilitate compliance with the conjugate centrosymmetry constraint in (4.23). In light of the condition cited above that $q_{IC} = q_{BC}$, the appropriate Gram–Schmidt procedure is

$$q_C = \frac{q_{BC}}{(q_{BC}^H C_I^H C_I q_{BC})} \tag{4.24a}$$

$$q_L' = q_{BL} - (q_C^H C_I^H C_I q_{BL}) q_C; \qquad q_L = \frac{q_L'}{(q_L'^H C_I^H C_I q_L')} \tag{4.24b}$$

$$q_R' = q_{BR} - (q_L^H C_I^H C_I q_{BR}) q_L - (q_C^H C_I^H C_I q_{BR}) q_C;$$

$$q_R = \frac{q_R'}{(q_R'^H C_I^H C_I q_R')}. \tag{4.24c}$$

Invoking the fact that $C_I^H C_I$ is Toeplitz–Hermitian, such that $\tilde{I}_3 C_I^H C_I \tilde{I}_3 = \{C_I^H C_I\}^*$, and the fact that q_{BL}, q_{BC}, and q_{BR} defined by (3.22) are each conjugate centrosymmetric, it is easy to show that q_L, q_C, and q_R constructed according to (4.24) are each conjugate centrosymmetric as well. Let $Q = [q_L \vdots q_C \vdots q_R]$ and $W_Q = C_I Q$. It follows that the columns of W_Q are orthonormal and conjugate centrosymmetric, i.e., W_Q satisfies the following two relationships:

$$W_Q^H W_Q = I_3; \qquad \tilde{I}_M W_Q = W_Q^*. \tag{4.25}$$

With $W_Q = C_I Q$ constructed according to step 1 above, the constrained LSE problem in (4.23) may be reformulated as

$$\underset{T_Q}{\text{Minimize}} \ \|W_B - C_I Q_I\|_F^2 = \|W_B - W_Q T_Q\|_F^2$$

$$\text{subject to:} \quad T_Q^H T_Q = T_Q T_Q^H = I_3. \tag{4.26}$$

As stated previously, what we have effectively done is to factor Q_I as QT_Q where Q is determined such that the columns of $C_I Q$ are orthonormal and T_Q is unitary. Since T_Q is unitary, it follows that the columns of $W_I = W_Q T_Q = \{C_I Q\} T_Q$ are orthonormal. In this manner, the constrained LSE problem defined by (4.23) is converted into the classical Procrustes rotation problem [20] defined by (4.26). One method of solving the Procrustes rotation problem defined by (4.26) involves the computation of the SVD of the 3×3 matrix $W_B^H W_Q$. Invoking the conjugate centrosymmetry of the columns of both W_B and W_Q, it follows that $W_B^H W_Q = W_B^H \tilde{I}_M \tilde{I}_M W_Q = W_B^T W_Q^* = [W_B^H W_Q]^*$. This proves that $W_B^H W_Q$ is a real-valued 3×3 matrix. This reduces computation somewhat as only real computations are required in computing the SVD of $W_B^H W_Q$. The solution to (4.26) is then as follows. If $W_B^H W_Q = U \Sigma V^T$ is the SVD, then $T_Q = UV^T$. Of course, T_Q is a 3×3 real-valued, orthogonal matrix. Thus, it easily follows that the columns of $W_I = W_Q T_Q$ are conjugate centrosymmetric since $\tilde{I}_M W_I = \tilde{I}_M W_Q T_Q = W_Q^* T_Q = W_I^*$. Thus, $b_I(u) = W_I^H a(u)$ is a real-valued, 3×1 vector as desired.

A summary of the procedure for constructing W_I is delineated below. Note that the first step in this procedure is the construction of w_{IC}. Five procedures for constructing w_{IC} were presented. The Gram–Schmidt based procedure is specifically cited in the prescription below.

C. Summary of Method for Constructing W_I (Gram–Schmidt Option for w_{IC})

1a) Construct orthonormal basis for span $\{a(u_c + 2/M; M), a(u_c - 2/M; M), a(u_{I1}; M), \cdots, a(u_{IK}; M)\}$.

1b) Construct w_{IC} by subtracting from $a(u_c; M)$ its components on this subspace.

2a) Form the length $M - 2$ sequence $\{c_I\}$ by deconvolving the length 3 sequence $\{q_{BC}\}$, defined by (3.20), out of the length M sequence $\{w_{IC}\}$.

2b) Construct $M \times 3$ banded Toeplitz matrix C_I according to (4.4).

3a) Construct orthonormal basis $\{q_L, q_C, q_R\}$ for 3-D Hilbert space defined by $\langle x, y \rangle = x^H C_I^H C_I y$ according to (4.24) with initial basis $\{q_{BL}, q_{BC}, q_{BR}\}$ defined by (3.22).

3b) With $Q = [q_L \vdots q_C \vdots q_R]$, construct $W_Q = C_I Q$.

4a) Compute 3×3 real-valued SVD: $W_B^H W_Q = U \Sigma V^T$.

4b) Form $T_Q = UV^T$.

5) $W_I = W_Q T_Q = C_I Q T_Q$ and $Q_I = Q T_Q$.

With W_I and Q_I determined according to this procedure, the only changes to the 3D-BDMUSIC algorithm outlined previously in Section III is that W_I replace W_B in step 1) and that $e_*(z)$ in step 4) be the second-order polynomial associated with the vector $e^* = \{Q_I v\}^* = Q_I^* v$, where v is the EVEC of Re $\{\hat{R}_{bb}\}$ associated with the "smallest" EV.

V. Frequency Diversity

Advances in radar technology have progressed to the point where the use of frequency diversity in tracking systems has become increasingly more commonplace [8], [11], [21]. Depending on the system hardware, the pulses at the various frequencies may be transmitted simultaneously and/or in rapid succession corresponding to frequency hopping. There are a lot of advantages to employing frequency diversity for tracking purposes. For our purposes here, the use of multiple frequencies allows us to achieve a large effective signal-to-interference plus noise ratio (SINR). This is accomplished by coherently combining the additive component of the beamspace correlation matrix at each frequency associated with the two signals of interest; the additive components of the beamspace correlation matrix at each frequency due to interference and receiver noise are incoherently combined. (In the case of low-angle radar tracking, the two signals of interest are the direct and specular path signals.) The coherent combination of the signal-only (no noise and no interference) component of the beamspace correlation matrix at each frequency is accomplished through the use of focusing matrices in accordance with the coherent signal subspace (CSS) processing method of Wang and Kaveh [13], [14]. Another advantage of frequency diversity is that it inherently produces diversity in the phase difference occurring at the center of the array which, when exploited by the CSS processing, diminishes the sensitivity of 3D-BDMUSIC to the phase difference at any one frequency. This is important for the following reasons. Although the use of spatial smoothing [15] prior to the transformation to 3-D beamspace theoretically eliminates the aforementioned problems with $\Delta\Psi(n) = 0°$ and $\Delta\Psi(n)$

$= 180°$ in the single snapshot or coherent case, the case of $\Delta\Psi(n) = 180°$ remains problematic in practice. This is due to the severe signal cancellation occurring across a large portion of the array when $\Delta u = |u_1 - u_2|$ is a fraction of a beamwidth, giving rise to a low effective SNR. Multifrequency operation with CSS processing diminishes the pejorative effect of a 180° phase difference at any one transmission frequency.

A multifrequency version of 3D-BDMUSIC incorporating CSS based on Butler matrix beamforming was developed in [10]–[12]. The contribution here is simply an adaptation of that algorithm incorporating interference cancellation. Only a brief explanation is provided; details may be found in [10], [12]. A discussion of multifrequency operation requires the introduction of some notation. The transmission frequencies are denoted f_j, $j = 1, \cdots, J$, where J is the total number of such frequencies. f_0 denotes the frequency for which the M elements of the array are spaced by a half-wavelength; f_0 may or may not be one of the transmission frequencies. Let $\boldsymbol{W}_I(f_j)$ denote the $M_j \times 3$ beamformer to be applied to each of $M - M_j + 1$ identical subarrays of $M_j < M$ contiguous elements at frequency f_j. In fact, it may well be that $M_j = M$, $j = 1, \cdots, J$, corresponding to no spatial smoothing at any frequency. However, it may be desirable to perform a small amount of spatial smoothing at each frequency to further diminish the sensitivity to the phase difference at any one frequency. In addition, as in the case of multifrequency 3D-BDMUSIC employing Butler matrix beamforming [10]–[12], operating with an effective subaperture equal to that associated with a subarray of M_j elements at frequency f_j leads to a criterion for the selection of transmission frequencies which makes the job of coherently combining the signal-only component of $\tilde{\boldsymbol{R}}_{bb}(f_j)$, the "spatially smoothed" beamspace correlation matrix formed at f_j, a very simple procedure. This criterion will be discussed shortly.

The element space manifold vector associated with frequency f_j and a subarray of M_j contiguous elements is denoted $\boldsymbol{a}(u; f_j, M_j)$. $\boldsymbol{a}(u; M)$ in (3.2), now denoted $\boldsymbol{a}(u; f_0, M)$, is easily generalized for arbitrary frequencies of operation and subarrays of length M_j:

$$\boldsymbol{a}(u; f_j, M_j) = \left[\exp\left(-j\pi \frac{M_j - 1}{2}\frac{f_j}{f_0}u\right), \exp\left(-j\pi \frac{M_j - 3}{2}\frac{f_j}{f_0}u\right), \cdots, \exp\left(j\pi \frac{M_j - 3}{2}\frac{f_j}{f_0}u\right), \exp\left(j\pi \frac{M_j - 1}{2}\frac{f_j}{f_0}u\right)\right]^T. \tag{5.1}$$

Consider the $M_j \times 3$ matrix beamformer

$$\boldsymbol{W}_B(f_j) = \frac{1}{\sqrt{M_j}}\left[\boldsymbol{a}\left(u_c - \frac{f_0}{f_j}\frac{2}{M_j}; f_j, M_j\right) \vdots \boldsymbol{a}(u_c; f_j, M_j) \vdots \boldsymbol{a}\left(u_c + \frac{f_0}{f_j}\frac{2}{M_j}; f_j, M_j\right)\right] \quad j = 1, \cdots, J. \tag{5.2}$$

Given the definition of $\boldsymbol{a}(u; f_j, M_j)$ in (5.1), it is easily verified that the columns of $\boldsymbol{W}_B(f_j)$ are mutually orthonormal. For each f_j, $j = 1, \cdots, J$, the $M_j \times 3$ matrix beamformer $\boldsymbol{W}_I(f_j)$ for interference cancellation purposes is constructed according to an optimization problem similar to (4.23):

$$\begin{aligned}
&\underset{\boldsymbol{Q}_I(f_j)}{\text{Minimize}} \ \|\boldsymbol{W}_B(f_j) - \boldsymbol{W}_I(f_j)\|_F^2 \\
&\quad = \|\boldsymbol{W}_B(f_j) - \boldsymbol{C}_I(f_j)\,\boldsymbol{Q}_I(f_j)\|_F^2 \\
&\text{subject to:} \quad \boldsymbol{W}_I^H(f_j)\,\boldsymbol{W}_I(f_j) \\
&\qquad = \boldsymbol{Q}_I^H(f_j)\{\boldsymbol{C}_I^H(f_j)\,\boldsymbol{C}_I(f_j)\}\boldsymbol{Q}_I(f_j) = \boldsymbol{I}_3 \\
&\tilde{\boldsymbol{I}}_3\boldsymbol{W}_I(f_j) \\
&\qquad = \tilde{\boldsymbol{I}}_3\{\boldsymbol{C}_I(f_j)\,\boldsymbol{Q}_I(f_j)\} = \{\boldsymbol{C}_I(f_j)\,\boldsymbol{Q}_I(f_j)\}^* = \boldsymbol{W}_I^*(f_j)
\end{aligned} \tag{5.3}$$

where $\boldsymbol{C}_I(f_j)$ is an $M_j \times 3$ banded-Toeplitz matrix of the form in (4.4). $\boldsymbol{C}_I(f_j)$ may be determined for each frequency f_j, $j = 1, \cdots, J$, by any of the five methods described previously for single frequency operation, appropriately adapted invoking the form of $\boldsymbol{a}(u; f_j, M_j)$ in (5.1). For the procedure based on the interference polynomial, the appropriately modified interference polynomial for f_j, $j = 1, \cdots, J$, is

$$i_j(z) = \alpha_j\left(z - \exp\left(j\pi\frac{f_j}{f_0}u_{I1}\right)\right)\cdot\left(z - \exp\left(j\pi\frac{f_j}{f_0}u_{I2}\right)\right)\cdots\left(z - \exp\left(j\pi\frac{f_j}{f_0}u_{IK}\right)\right) \quad j = 1, \cdots, J. \tag{5.4}$$

It should be kept in mind that implicit in the prescription in (5.3) is that the beamformers $\boldsymbol{W}_I(f_j)$, $j = 1, \cdots, J$, must satisfy the null constraints $\boldsymbol{W}_I^H(f_j)\,\boldsymbol{a}(u_{Ik}; f_j, M_j) = 0_3$, $k = 1, 2, \cdots, K$. In addition, for each frequency, the respective beams formed by each of the three columns of $\boldsymbol{W}_I(f_j)$ must have $M_j - 3$ nulls in common.

Having constructed $\boldsymbol{W}_I(f_j)$ for each transmission frequency, the first step in multifrequency 3D-BDMUSIC incorporating both CSS and interference cancellation is to form $\tilde{\boldsymbol{R}}_{bb}(f_j)$ as follows. Decompose the overall array into $M - M_j + 1$ overlapping subarrays of M_j contiguous elements. $\boldsymbol{W}_I(f_j)$ is applied to each subarray, and $\tilde{\boldsymbol{R}}_{bb}(f_j)$ is

formed as the arithmetic mean of the outer products of the $(M - M_j + 1)$ 3 × 1 beamspace snapshot vectors thus created. This is done for each of the J transmission frequencies. The CSS averaging is then achieved by the construction of Re $\{\bar{R}_{bb}\} = 1/J \sum_{j=1}^{J} T_j^k \tilde{R}_{bb}(f_j) T_j^{kT}$, where the focusing matrix T_j^k "translates" the signal-only component of $\tilde{R}_{bb}(f_j)$ to f_k, where $f_k \in \{f_1, f_2, \cdots, f_J\}$. Let $b_I(u; f_j) = W_I^H(f_j)\, a(u; f_j, M_j), j = 1, \cdots, J$, and $B_I(f_j) = [b_I(u_1; f_j) \vdots b_I(u_2; f_j)], j = 1, \cdots, J$. The focusing matrices must satisfy $B_I(f_k) = T_j^k B_I(f_j), j = 1, \cdots, J$. Of course, the notation is such that $T_k^k = I_3$. Note that since $b_I(u; f_j)$ is a real-valued 3 × 1 manifold vector, T_j^k is a real-valued 3 × 3 matrix, $j = 1, \cdots, J$. Once the CSS averaging has been performed, v is computed as the "smallest" generalized EVEC of the 3 × 3 pencil $\{\text{Re}\,\{\bar{R}_{bb}\}, \bar{T}\}$, where $\bar{T} = 1/J \sum_{i=1}^{J} T_i^k T_i^{kT}$. Finally, $z_1 = e^{j\pi u_1}$ and $z_2 = e^{j\pi u_2}$ are estimated as the two roots of $e_*(z)$, the quadratic polynomial associated with the conjugate of the 3 × 1 vector $e = Q(f_k) v$.

Construction of the focusing matrices T_j^k, $j = 1, \cdots, J$, in fact requires knowledge of u_1 and u_2, i.e., the angles we are trying to estimate. As a consequence, Wang and Kaveh [13], [14] propose an iterative procedure which commences with an initial set of focusing matrices based on some coarse estimates of the angles. One possibility for initialization is to take the pointing angle of the center beam u_c as an estimate of both angles. Proceeding with the initial set of focusing matrices yields updated estimates of the angles corresponding to the first iteration. The new pair of angles are used to construct an updated set of focusing matrices which, in turn, yield the estimates of the angles at the second iteration. The procedure is then iterated until the absolute value of the difference between respective angle estimates obtained at the $(k + 1)$th and kth iterations is less than some threshold for both signals. A number of methods for constructing the focusing matrices have been proposed [13], [14].

In [10]–[12] it was shown that the need for focusing matrices in multifrequency 3D-BDMUSIC based on Butler matrix beamforming may be eliminated if the transmission frequencies, $f_j, j = 1, \cdots, J$, and corresponding subarray lengths, $M_j, j = 1, \cdots, J$, are selected such that the product $f_j M_j$ is the same for each frequency, i.e., $f_j M_j = \alpha, j = 1, \cdots, J$. The following justification is provided. In the case of Butler matrix beamforming at each frequency with $W_B(f_j), j = 1, \cdots, J$, defined by (5.2), the corresponding beamspace manifold vector over the angular region $u_c - (f_0/f_j)(6/M_j) < u < u_c + (f_0/f_j)(6/M_j)$ may be approximated as

$$
\begin{aligned}
b(u; f_j) &= W_B^H(f_j)\, a(u; f_j, M_j) \\
&= \frac{1}{M_j} \left[\frac{\sin\left(M_j \frac{\pi}{2} \frac{f_j}{f_0}\left(u - u_c + \frac{f_0}{f_j}\frac{2}{M_j}\right)\right)}{\sin\left(\frac{\pi}{2}\frac{f_j}{f_0}\left(u - u_c + \frac{f_0}{f_j}\frac{2}{M_j}\right)\right)}, \right. \\
&\qquad \frac{\sin\left(M_j \frac{\pi}{2} \frac{f_j}{f_0}(u - u_c)\right)}{\sin\left(\frac{\pi}{2}\frac{f_j}{f_0}(u - u_c)\right)}, \\
&\qquad \left. \frac{\sin\left(M_j \frac{\pi}{2} \frac{f_j}{f_0}\left(u - u_c - \frac{f_0}{f_j}\frac{2}{M_j}\right)\right)}{\sin\left(\frac{\pi}{2}\frac{f_j}{f_0}\left(u - u_c - \frac{f_0}{f_j}\frac{2}{M_j}\right)\right)} \right]^T \\
&\approx \frac{f_0}{M_j f_j} \left[\frac{\sin\left(\frac{\pi}{2}\frac{M_j f_j}{f_0}\left(u - u_c + \frac{f_0}{f_j}\frac{2}{M_j}\right)\right)}{\left(\frac{\pi}{2}\left(u - u_c + \frac{f_0}{f_j}\frac{2}{M_j}\right)\right)}, \right. \\
&\qquad \frac{\sin\left(\frac{\pi}{2}\frac{M_j f_j}{f_0}(u - u_c)\right)}{\left(\frac{\pi}{2}(u - u_c)\right)}, \\
&\qquad \left. \frac{\sin\left(\frac{\pi}{2}\frac{M_j f_j}{f_0}\left(u - u_c - \frac{f_0}{f_j}\frac{2}{M_j}\right)\right)}{\left(\frac{\pi}{2}\left(u - u_c - \frac{f_0}{f_j}\frac{2}{M_j}\right)\right)} \right]^T . \qquad (5.5)
\end{aligned}
$$

This approximation is tantamount to approximating the respective array patterns formed by each of the three columns of $W_B(f_j)$ defined by (5.2) as a sinc function in the vicinity of the respective mainlobe and first sidelobes. It is thus apparent that if $f_j M_j = \alpha, j = 1, \cdots, J$, the beamspace manifold vector $b(u; f_j)$ is the same for each transmission frequency. Hence, CSS averaging is simply accomplished by summing the spatially smoothed beamspace correlation matrices formed at each frequency. This represents a dramatic simplification.

With regard to interference cancellation, note that construction of $W_I(f_j)$ for each frequency according to the prescription in (5.3) dictates that $W_I(f_j)$ be as "close" as possible to $W_B(f_j)$, in the sense of minimizing the Frobenius norm of the difference between the two, while complying with the null constraints $W_I^H(f_j)\, a(u_{Ik}; f_j, M_j) = 0_3, k = 1, 2, \cdots, K$. As a consequence, it is easily argued that for each frequency $b_I(u; f_j) = W_I^H(f_j)\, a(u; f_j, M_j) \approx b(u) = W_B^H(f_j)\, a(u; f_j, M_j)$ over the angular region $u_c - (f_0/f_j)(6/M_j) < u < u_c + (f_0/f_j)(6/M_j)$. It follows from previous arguments then that if the transmission frequencies satisfy $f_j M_j = \alpha, j = 1, \cdots, J$, $b_I(u; f_j) = W_I^H(f_j)\, a(u; f_j, M_j)$ is the same for each frequency over the angular region $u_c - (f_0/f_j)(6/M_j) < u < u_c + (f_0/f_j)(6/M_j)$. As the case with Butler matrix beamforming [10]–[12], CSS averaging is then simply accomplished by summing $\tilde{R}_{bb}(f_j), j = 1, \cdots, J$. Also,

this result implies that $\boldsymbol{Q}_I(f_j)$ must be approximately the same for each frequency. Thus, the simplified version of multifrequency 3D-BDMUSIC incorporating both CSS and interference cancellation for the case where the transmission frequencies satisfy $f_j M_j = \alpha, j = 1, \cdots, J$, is as follows.

With $\boldsymbol{W}_I(f_j)$ constructed for each transmission frequency in accordance with (5.3), form $\tilde{\boldsymbol{R}}_{bb}(f_j)$, $j = 1, \cdots, J$, as described above. $\boldsymbol{v}$ is then computed as the "smallest" EVEC of Re $\{\tilde{\boldsymbol{R}}_{bb}\} = 1/J \sum_{j=1}^{J} \tilde{\boldsymbol{R}}_{bb}(f_j)$. (Note that this step exploits the fact that $\boldsymbol{W}_I^H(f_j)\, \boldsymbol{W}_I(f_j) = \boldsymbol{I}_3, j = 1, \cdots, J$, which avoids a generalized EVD and estimation of the noise power at each frequency.) $z_1 = e^{j\pi u_1}$ and $z_2 = e^{j\pi u_2}$ are then estimated as the two roots of $e_*(z)$, the quadratic polynomial associated with the conjugate of the 3×1 vector $\boldsymbol{e} = \boldsymbol{Q}(f_k)\boldsymbol{v}$, where f_k is any one of the transmission frequencies. This form of the algorithm will be used in the simulation presented in Section VI.

VI. Computer Simulations

Computer simulations were conducted to ascertain the performance of both single frequency and multifrequency 3-D BDMUSIC incorporating interference cancellation in a simulated low-angle radar tracking environment with jamming. The following parameters were common to all test cases. First, the array employed was linear consisting of $M = 21$ elements uniformly spaced by a half-wavelength at f_0. The nominal 3-dB beamwidth for this array is $2/21$ rads $= 5.46°$. The two signals of interest, the direct and specular path signals, were angularly located at $\theta_1 = 1.5°$ and $\theta_2 = -1°$, respectively, corresponding to an angular separation of 0.46 beamwidths or roughly a half-beamwidth. The noise was additive, spatially white, and uncorrelated with the direct and specular path signals, and with the interfering signals as well. The SNR of the direct path signal was 20 dB (per element). The ratio of the amplitude of the specular path signal to that of the direct path signal ρ was 0.9. In the case of single frequency operation at f_0, corresponding to the simulations presented in Figs. 2–5, each independent trial involved the execution of 3D-BDMUSIC incorporating interference cancellation given a single snapshot of data, $N = 1$. For each simulation example, the respective performance for five different values of $\Delta\Psi$, the phase difference between the direct and specular path signals at the center element, was examined. Multifrequency operation with three frequencies satisfying $f_j M_j =$ constant, $j = 1, 2, 3$, is examined in Fig. 6. In this case, each independent trial involved the execution of the simplified multifrequency version of 3D-BDMUSIC incorporating interference cancellation summarized at the end of Section V given a single snapshot of data, $N = 1$, at each of the three frequencies. Finally, in all cases, sample means (SMEAN's) and sample standard deviations (SSTD's) were computed from the results of 100 independent trials.

In the single snapshot case, single frequency 3D-BDMUSIC incorporating interference cancellation

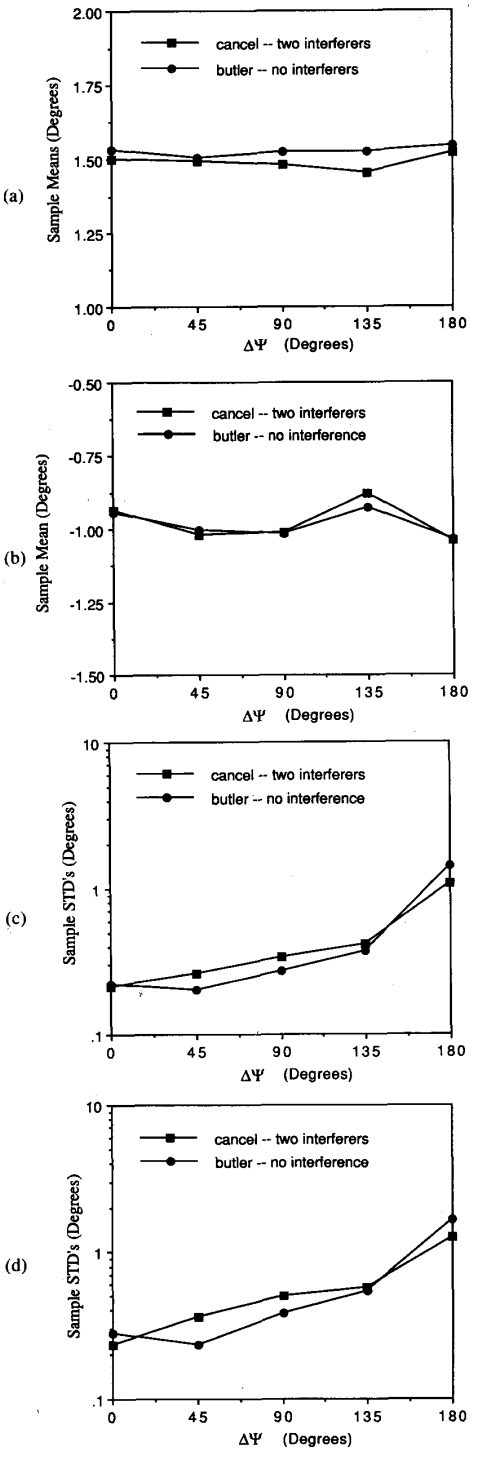

Fig. 2. Performance comparison: 3D-BDMUSIC with no interference and Butler matrix beamforming versus 3D-BDMUSIC with two interferers and ICMBF. $M = 21$ elements and $N = 1$ snapshot. Direct path: $\theta_1 = 1.5°$ and SNR = 20 dB. Specular path: $\theta_2 = -1°$ and $\rho = 0.9$. Interferers: $\theta_{I1} = 13.5°$ and $\theta_{I2} = 25°$ with SNR = 20 dB each (SIR = 0 dB). SMEAN's/SSTD's computed from 100 independent trials. (a) Direct path sample means. (b) Specular path sample means. (c) Direct path sample STD's. (d) Specular path sample STD's.

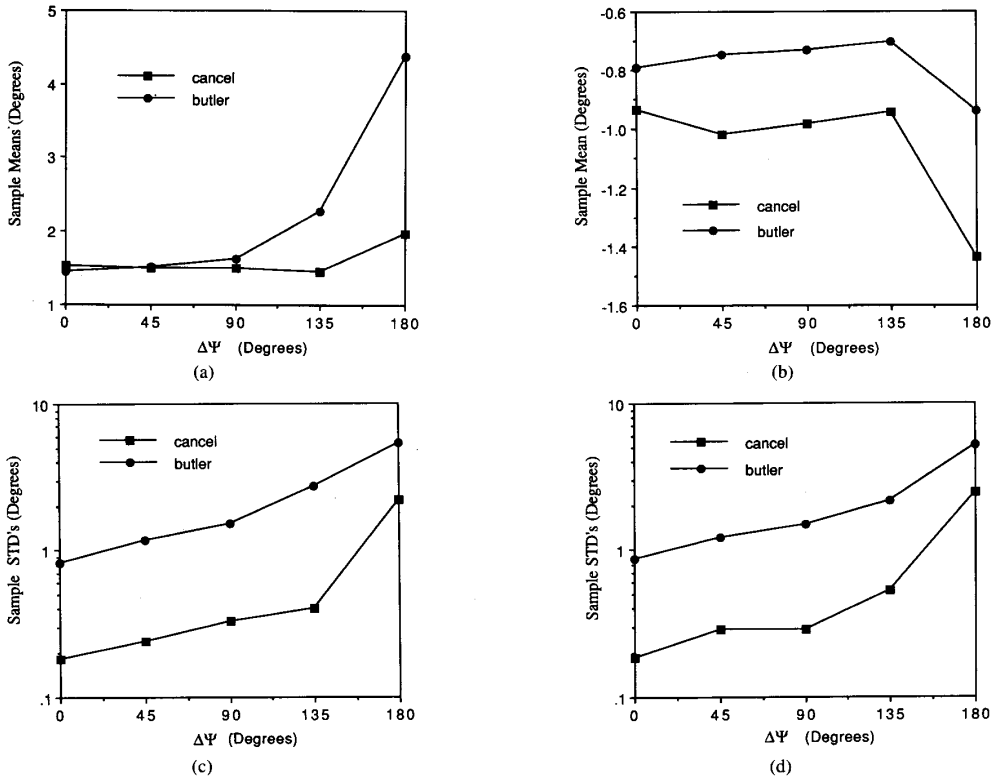

Fig. 3. Performance comparison: 3D-BDMUSIC with Butler beamforming versus 3D-BDMUSIC with ICMBF. Simulations parameters same as those described in caption to Fig. 2 except $\theta_{I1} = 15°$ and $\theta_{I2} = 28°$. (a) Direct path sample means. (b) Specular path sample means. (c) Direct path sample STD's. (d) Specular path sample STD's.

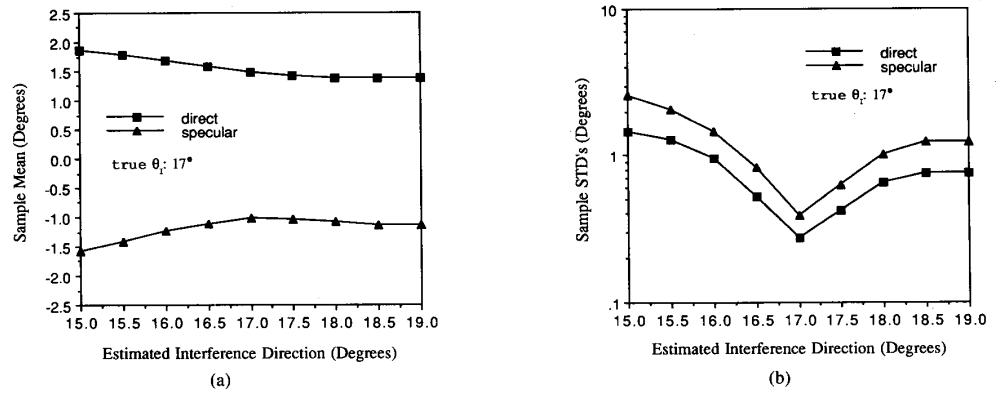

Fig. 4. Sensitivity of 3D-BDMUSIC with ICMBF to error in estimated interference angle. Simulations parameters same as those described in caption to Fig. 2 except single interferer located at $\theta_{I1} = 17°$ with SNR = 20 dB (SIR = 0 dB). (a) Sample means. (b) Sample STD's.

does not work properly if $\Delta\Psi(n)$ is either 0° or 180° as discussed previously. In the case of 3D-BDMUSIC with $M \times 3$ Butler matrix beamforming, this problem is averted by employing spatial smoothing combined with symmetrization [12]. In this mode of operation, the 2-D parameter estimation problem is decomposed into two successive 1-D parameter estimation problems. That is, instead of simultaneously estimating both u_1 and u_2, we first estimate the bisector angle $u_B = 1/2\{u_1 + u_2\}$ and then, as a second step, estimate $\delta = |u_1 - u_B| = |u_2 - u_B|$.

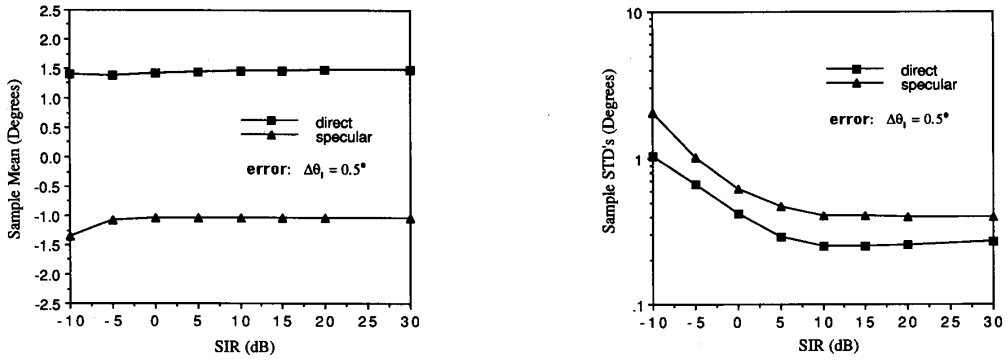

(a) (b)

Fig. 5. Performance of 3D-BDMUSIC with ICMBF as a function of SIR with an interference angle estimation error of 0.5°. Simulations parameters same as those described in caption to Fig. 2 except single interferer located at $\theta_{I1} = 17°$. Estimated interference angle: $\hat{\theta}_{I1} = 17.5°$. (a) Sample means. (b) Sample STD's.

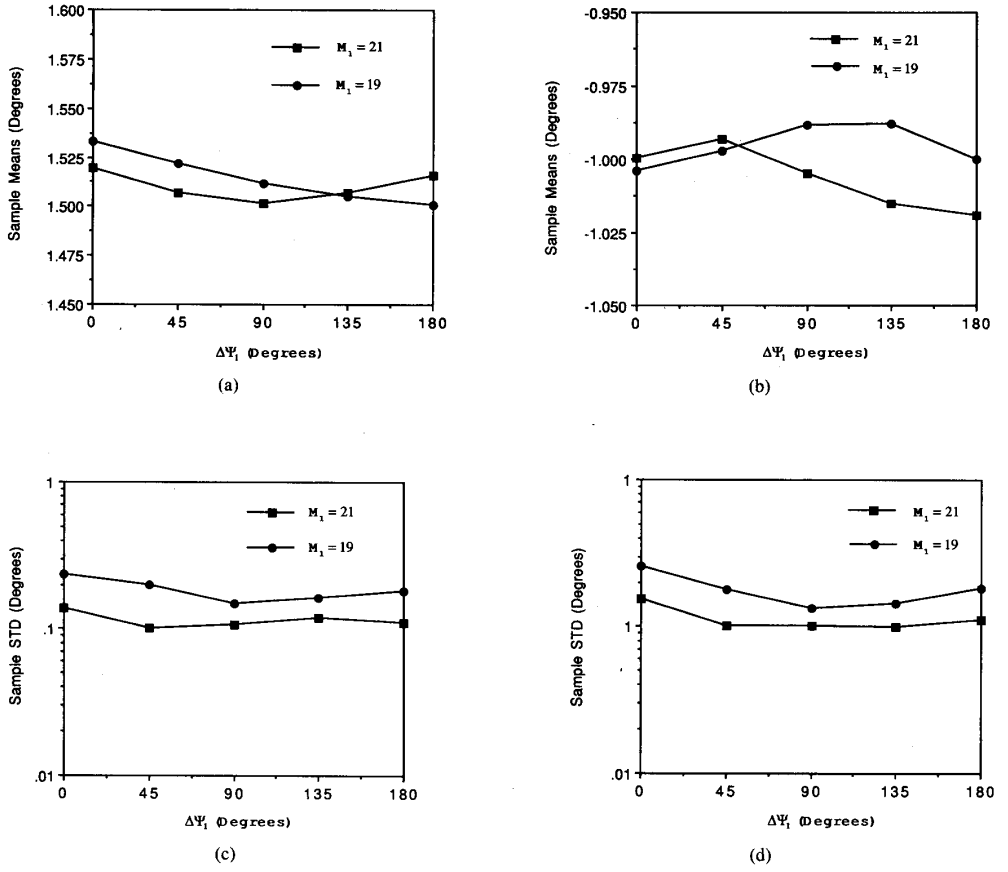

(a) (b)

(c) (d)

Fig. 6. Performance of multifrequency 3D-BDMUSIC with ICMBF. Simulations parameters same as those described in caption to Fig. 4 except $J = 3$ frequencies employed. f_0: frequency for which elements spaced by half-wavelength. $\Delta\Psi_1$: phase difference at aperture center at $f_1 = f_0$. Case 1 ($M_1 = 21$): $f_1 = f_0$, $f_2 = \frac{21}{19}f_0$ and $f_3 = \frac{21}{17}f_0$, Case 2 ($M_1 = 19$): $f_1 = f_0$, $f_2 = \frac{19}{21}f_0$ and $f_3 = \frac{19}{17}f_0$. (a) Direct path sample means. (b) Specular path sample means. (c) Direct path sample STD's. (d) Specular path sample STD's.

Simulations have indicated that this procedure, referred to as the spatial smoothing/symmetrization version of 3D-BDMUSIC, is less sensitive to the reduction in aperture length incurred with spatial smoothing [12]. This refinement to 3D-BDMUSIC is easily adapted for 3D-BDMUSIC incorporating interference cancellation and was employed in the simulation associated with Figs. 2–5.

In the first simulation example, the interference scenario consisted of $K = 2$ interferers angularly located at $\theta_{I1} = 13.5°$ and $\theta_{I2} = 25°$. Each of these interferers had the same signal strength, i.e., the same SNR, as the direct path signal. Fig. 1(a) displays the three beams generated by the 21×3 Butler matrix beamformer $\boldsymbol{W}_B$ with a center pointing angle of $\theta_c = 0°$. Note that the three beams have $21 - 3 = 18$ nulls in common. Also note that the angular position of the first interferer is the location of the peak of the largest sidelobe of the beam pointed to 5.46°, and the location of the respective peaks of the second and third largest sidelobes of the beams pointed to 0° and −5.46°, respectively, as well. The angular position of the second interferer is also located at a peak of one of the sidelobes of each of the three beams. In contrast to Fig. 1(a), Fig. 1(b) displays the three beams generated by the interference cancellation matrix beamformer $\boldsymbol{W}_I$ constructed according to the method outlined at the end of Section IV with the actual (no estimation error) values of θ_{I1} and θ_{I2}. Note that by design the three beams have 18 nulls in common with two of the nulls located at $\theta_{I1} = 13.5°$ and $\theta_{I2} = 25°$.

The simulation results presented in Fig. 2 compare the performance of 3D-BDMUSIC employing $\boldsymbol{W}_I$ in this interference environment with that of 3D-BDMUSIC employing $\boldsymbol{W}_B$ ($\theta_c = 0°$) in an "interference-free" environment. Since in the former case the nulls are exactly aligned with the actual interference directions, comparable performance is expected and is indeed obtained. Note that in either case, poor performance is obtained with $\Delta\Psi = 180°$ due to the substantial signal cancellation occurring across the array under these conditions. Overall, however, the performance of 3D-BDMUSIC with perfect interference cancellation is slightly worse than that achieved in the no interference case with $\boldsymbol{W}_B$. This may be attributed to a slight drop in the average gain in the direction of the direct and specular path signals associated with the three beams formed by $\boldsymbol{W}_I$ relative to that associated with the three beams formed by $\boldsymbol{W}_B$. The performance gradually deteriorates as the location of an interferer, and hence, the corresponding null, approaches the angular locations of the direct and specular path signals.

The simulation results plotted in Figs. 3 and 7 illustrate the poor performance of 3D-BDMUSIC employing Butler matrix beamforming in the presence of interference. In order to achieve a SSTD for the estimates of the direct path angle for $\Delta\Psi = 90°$ no greater than half the angular separation between the direct and specular path signals, the interference locations were moved from the positions in the first simulation example to $\theta_{I1} = 15°$ and $\theta_{I2} = 28°$. The locations of these interferers relative to the sidelobes of the three beams formed by $\boldsymbol{W}_B$ with $\theta_c = 0°$ is depicted in Fig. 7(a). As before, each interferer had the same power as the direct path signal. Observing Fig. 3, it is noted that even in the best case of $\Delta\Psi = 0°$, the SSTD of the direct path angle is 0.8°. For comparison, the performance of 3D-BDMUSIC employing $\boldsymbol{W}_I$ constructed according to the method outlined at the end of Section IV with the true interference directions of $\theta_{I1} = 15°$ and $\theta_{I2} = 28°$ is presented in Fig. 3 as well. Fig. 7(b) displays the three beams generated by the $\boldsymbol{W}_I$ thus obtained. Except for the $\Delta\Psi = 180°$ case, the SSTD of the estimates obtained with this $\boldsymbol{W}_I$ is roughly an order of magnitude less than that obtained with $\boldsymbol{W}_B$.

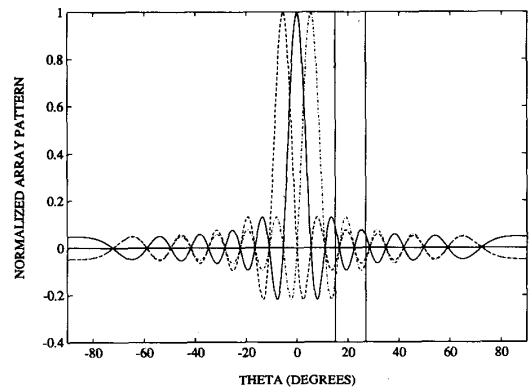

(a)

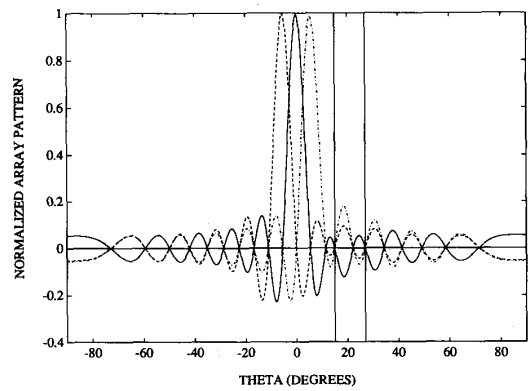

(b)

Fig. 7. Same as caption to Fig. 1 except $\theta_{I1} = 15°$ and $\theta_{I2} = 28°$. (a) Butler matrix beamforming. (b) Interference cancellation matrix beamforming.

An indication of the sensitivity of 3D-BDMUSIC incorporating interference cancellation to errors in the estimated interference directions may be gleaned from observing the simulation results plotted in Figs. 4 and 5. The scenario for these two simulation examples consisted of a single interferer located at $\theta_{I1} = 17°$. Fig. 4 displays the performance of 3D-BDMUSIC employing an interference cancellation matrix beamformer $\boldsymbol{W}_I$ constructed according to the method outlined at the end of Section IV

for various estimates of θ_{I1}. For this example, the interferer had the same power as the direct path signal. For an estimation error of fairly large magnitude equal to 0.5°, the SSTD of the direct path angle rises from the minimum value of 0.27° at $\hat{\theta}_{I1} = \theta_{I1} = 17°$, to 0.52° at $\hat{\theta}_{I1} = 16.5°$, and 0.42° at $\hat{\theta}_{I1} = 17.5°$. Note that it should not be expected that the SSTD will keep rising as the estimation error increases as it is possible for one of the other common null locations to eventually line up with the true interference direction. In generating the statistics plotted in Fig. 5, the estimated interference direction was held fixed at $\hat{\theta}_{I1} = 17.5°$, while the strength of the interfering signal at $\theta_{I1} = 17°$ was varied. Relative to the strength of the direct path signal, the signal-to-interference ratio (SIR) was varied from -10 to 30 dB in 5-dB steps. As expected, the pejorative effect of the interferer diminishes as the SIR increases, despite the estimation error of 0.5°. In fact, for this particular estimation error, the effect of the interferer appears to be negligible once the SIR reaches 10 dB.

The simulation results presented in Fig. 6 illustrate the excellent performance of the computationally simplistic version of multifrequency 3D-BDMUSIC incorporating interference cancellation for frequencies satisfying $f_j M_j =$ constant, where $M_j \leq M$, $j = 1, \cdots, J$. Two different simulation experiments were conducted, denoted case 1 and case 2. In both cases, the number of transmission frequencies was $J = 3$ with one of these equal to f_0. Also, in both cases the interference scenario consisted of $K = 2$ interferers located at $\theta_{I1} = 15°$ and $\theta_{I2} = 28°$ with each interferer having the same strength as the direct path signal at each transmission frequency. Arbitrarily assign $f_1 = f_0$ such that M_1 denotes the number of elements comprising the subarrays over which spatial smoothing is performed at f_0. In case 1, $M_1 = 21$ corresponding to no spatial smoothing and, hence, use of the full aperture at f_0. This automatically dictates that the other two frequencies satisfy $f_j M_j = f_1 M_1 = 21 f_0$, or $f_j = (21/M_j) f_0$, $j = 2, 3$, where M_j is an integer strictly less than 21. The specific selections were $M_2 = 19$ and $M_3 = 17$ such that the three transmission frequencies for case 1 were $f_1 = f_0$, $f_2 = (21/19) f_0 = 1.105 f_0$, and $f_3 = (21/17) f_0 = 1.235 f_0$. In case 2, $M_1 = 19$ dictating that the other two frequencies satisfy $f_j M_j = f_1 M_1 = 19 f_0$, or $f_j = (19/M_j) f_0$, $j = 2, 3$, where M_j is an integer less than or equal to 21. The specific selections were $M_2 = 21$ and $M_3 = 17$ such that the three transmission frequencies for case 2 were $f_1 = f_0$, $f_2 = (19/21) f_0 = 0.905 f_0$, and $f_3 = (19/17) f_0 = 1.117 f_0$.

For each of the two cases, cases 1 and 2, a single snapshot was collected at each of the three transmission frequencies. For each frequency, f_j, $j = 1, 2, 3$, a suitably constructed interference cancellation matrix beamformer $\boldsymbol{W}_I(f_j)$ of dimension $M_j \times 3$ was applied to each of $M - M_j + 1$ identical subarrays of M_j elements. The outer products of the $(M - M_j + 1)$ 3×1 beamspace snapshot vectors thus created were averaged to form $\tilde{\boldsymbol{R}}(f_j)$, $j = 1, 2, 3$. $\boldsymbol{v}$ was then computed as the "smallest" EVEC of the 3×3 matrix $\mathrm{Re}\{\tilde{\boldsymbol{R}}_{bb}\} = \frac{1}{3}\sum_{j=1}^{3} \tilde{\boldsymbol{R}}_{bb}(f_j)$. Finally, $z_1 = e^{j\pi u_1}$ and $z_2 = e^{j\pi u_2}$ were then estimated as the two roots of $e_*(z)$, the quadratic polynomial associated with the conjugate of the 3×1 vector $\boldsymbol{e} = \boldsymbol{Q}(f_1)\boldsymbol{v}$, where $f_1 = f_0$. SMEAN's and SSTD's of both the direct and specular path angle estimates obtained from this procedure were computed from the results of 100 independent trials for each of five different values of $\Delta\Psi_1$, the phase difference between the direct and specular path signals at the center element at $f_1 = f_0$. Note that the phase difference between the direct and specular path signals at the center element occurring at the other transmission frequencies was determined from that at $f_1 = f_0$ in accordance with the low-angle radar tracking model described by Barton [1]. The resulting statistics for both cases 1 and 2 are presented in Fig. 6. It is observed that in all cases the sample bias is less than 0.02° and the corresponding SSTD is less than 0.25°. Also, the performance is observed to be relatively insensitive to $\Delta\Psi_1$ or to the phase difference at the center element at any one frequency, in general. It is also observed that the frequencies associated with case 1 yielded better performance than those associated with case 2. For case 2 the SSTD's were all less than 0.15°. This is to be expected since the beamwidth for case 1, which is the same for each of the three frequencies due to judicious variation of the respective (effective) aperture lengths, is that associated with a linear array of 21 elements with half-wavelength spacing at f_0 and operating at f_0. On the other hand, the beamwidth for case 2 it is that associated with a linear array of 19 elements with half-wavelength spacing at f_0 and operating at f_0.

The selection of $f_1 = f_0$ and $M_1 = 21$ in case 1 automatically constrained the auxiliary frequencies to be greater than f_0, the frequency for which the elements are spaced by a half-wavelength. Although this ultimately lead to better performance than that achieved in case 2 where one of the frequencies was less than f_0, one should take into consideration the locations of the grating lobes. For a beam steered to broadside the first pair of grating lobes do not enter the visible region $-1 < u < 1$ as the frequency of transmission is increased until a frequency of $2f_0$. As the direct and specular path signals arrive near broadside, the grating lobe problem is not an issue of significant concern in the low-angle radar tracking application. However, for more general tracking purposes, the grating lobe problem associated with transmission frequencies significantly higher than f_0 becomes an issue of increasing concern the farther the direction of "look" departs from broadside.

VII. Summary

Judicious construction of an $M \times 3$ interference cancellation matrix beamformer enables one to nullify the effect of interferers and nevertheless estimate the respective bearings of two closely spaced targets via the computationally simple 3D-BDMUSIC algorithm with minor modification. A suitable MVDR based procedure for constructing the $M \times 3$ interference cancellation matrix

beamformer was developed based on the MVDR criterion which preserves those properties of $M \times 3$ Butler matrix beamforming critical to the computational simplicity of 3D-BDMUSIC. Computational simplicity in the case of multifrequency operation is maintained by coherent signal subspace processing according to the method of Wang and Kaveh. The performance of 3D-BDMUSIC in a simulated low-angle radar tracking environment under single snapshot conditions demonstrates the real-time ability of 3D-BDMUSIC to accurately estimate the respective bearings of two targets separated by less than a beamwidth in a hostile jamming environment.

REFERENCES

[1] D. K. Barton, "Low angle radar tracking," *Proc. IEEE*, vol. 62, pp. 687–704, June 1974.

[2] R. C. Davis, L. E. Brennan, and L. S. Reed, "Angle estimation with adaptive arrays in external noise fields," *IEEE Trans. Aerosp. Electron. Syst.*, vol. AES-12, no. 3, pp. 179–186, Mar. 1976.

[3] W. F. Gabriel, "A high-resolution target-tracking concept using spectral estimation techniques," NRL Rep. 6109, May 1984.

[4] W. D. White, "Low-angle radar tracking in the presence of multipath," *IEEE Trans. Aerosp. Electron. Syst.*, vol. AES-10, pp. 835–853, Nov. 1974.

[5] B. H. Cantrell, W. B. Gordon, and G. V. Trunk, "Maximum likelihood elevation angle estimation of radar targets using subapertures," *IEEE Trans. Aerosp. Electron. Syst.*, vol. AES-17, pp. 213–221, Mar. 1981.

[6] W. B. Gordon, "Improved three subaperture method for elevation angle estimation," *IEEE Trans. Aerosp. Electron. Syst.*, vol. AES-19, pp. 114–122, Jan. 1983.

[7] S. Haykin, "Radar array processing for angle-of-arrival estimation," in *Array Signal Processing*. Englewood Cliffs, NJ: Prentice-Hall, 1985, ch. 4.

[8] V. Kezys and S. Haykin, "Multifrequency angle-of-arrival estimation: An experimental evaluation," *Proc. SPIE Int. Soc. Opt. Eng.*, vol. 975, pp. 98–106, Aug. 1988.

[9] T. S. Lee and M. Zoltowski, "Beamspace domain ML based low angle radar tracking with an array of antennas," in *Dig. 1989 IEEE Int. Antennas Propagat. Symp.*, vol. II, June 1989, pp. 663–666.

[10] M. Zoltowski and T. S. Lee, "Maximum likelihood based sensor array signal processing in the beamspace domain for low angle radar tracking," *IEEE Trans. Signal Processing*, vol. 39, no. 3, pp. 656–671, Mar. 1991.

[11] M. Zoltowski and T. S. Lee, "Bearing estimation in beamspace employing frequency diversity," *Proc. SPIE Int. Soc. Opt. Eng.*, vol. 1152, pp. 277–287, Aug. 1989.

[12] T. S. Lee, "Beamspace domain ML based low-angle radar tracking with an array of antennas," Ph.D. dissertation, Purdue University, Dec. 1989.

[13] H. Wang and M. Kaveh, "Coherent single-subspace averaging for the detection and estimation of angles of arrival of multiple wide-band sources," *IEEE Trans. Acoust., Speech, Signal Processing*, vol. ASSP-33, pp. 823–831, Aug. 1985.

[14] H. Hung and M. Kaveh, "Focusing matrices for coherent signal-subspace processing," *IEEE Trans. Acoust., Speech, Signal Processing*, vol. ASSP-36, pp. 1272–1281, Aug. 1988.

[15] T. J. Shan, M. Wax, and T. Kailath, "On spatial smoothing for direction-of-arrival estimation of coherent signals," *IEEE Trans. Acoust., Speech, Signal Processing*, vol. 33, pp. 806–811, Aug. 1985.

[16] Y. Bresler, V. U. Reddy, and T. Kailath, "Optimum beamforming for coherent signal and interferences," *IEEE Trans. Acoust., Speech, Signal Processing*, vol. ASSP-36, no. 6, pp. 833–843, June 1988.

[17] R. O. Schmidt, "Multiple emitter location and signal parameter estimation," *IEEE Trans. Antennas Propagat.*, vol. AP-34, no. 3, pp. 276–281, Mar. 1986.

[18] Y. Bresler and A. Macovski, "Exact maximum likelihood parameter estimation of superimposed exponential signals in noise," *IEEE Trans. Acoust., Speech, Signal Processing*, vol. ASSP-34, no. 5, pp. 1081–1089, Oct. 1986.

[19] R. Roy and T. Kailath, "ESPRIT—estimation of signal parameters via rotational invariance techniques," *IEEE Trans. Acoust., Speech, Signal Processing*, vol. 37, pp. 984–995, July 1989.

[20] M. Zoltowski and D. Stavrinides, "Sensor array signal processing via a Procrustes rotations based eigenanalysis of the ESPRIT data pencil," *IEEE Trans. Acoust., Speech, Signal Processing*, vol. ASSP-37, pp. 832–861, June 1989.

[21] J. A. Adam, "Pinning defense hopes on AEGIS," *IEEE Spectrum*, pp. 24–27, June 1988.

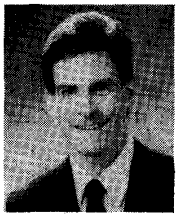

Michael D. Zoltowski (S'79–M'86) was born in Philadelphia, PA, on August 12, 1960. He received the B.S. and M.S. degrees in electrical engineering with highest honors from Drexel University in 1983 and the Ph.D. degree in systems engineering from the University of Pennsylvania in 1986.

From 1982 to 1986, he was an Office of Naval Research Graduate Fellow. In conjunction with his fellowship, he held a visiting research position at the Naval Research Laboratory in Washington, DC, during the summer of 1986. In fall 1986, he joined the faculty of Purdue University, where he currently holds a position of Assistant Professor of Electrical Engineering. During 1987, he held a position of Summer Faculty Research Fellow at the Naval Ocean Systems Center in San Diego, CA. His present research interests include sensor array signal processing, phased array radar, sonar, adaptive signal processing, higher order spectral analysis, and numerical linear algebra. He is a contributing author to *Adaptive Radar Detection and Estimation* (Wiley, 1991). He presently serves as a consultant to the General Electric Company.

Dr. Zoltowski is a member of Eta Kappa Nu, Tau Beta Pi, Phi Eta Sigma, and Phi Kappa Phi.

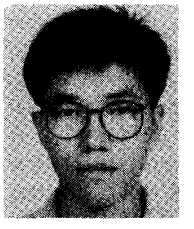

Ta-Sung Lee (S'88–M'89) was born in Taipei, Taiwan, Republic of China, on October 20, 1960. He received the B.S. degree from National Taiwan University in 1983, the M.S. degree from the University of Wisconsin at Madison in 1987, and the Ph.D. degree from Purdue University in 1989, all in electrical engineering.

From 1987 to 1989, he was a David Ross Graduate Research Fellow at Purdue University. In Spring 1990, he joined the faculty of National Chiao Tung University where he currently holds a position as Associate Professor in the Department of Communication Engineering. His research interests include sensor array signal processing, band-limited signal analysis, and adaptive equalization.